ACS Partner Journal

CHEMICAL & BIOMEDICAL IMAGING

pubs.acs.org/ChemBioImaging

Review

Tracing the Chromatin: From 3C to Live-Cell Imaging

Published as part of Chemical & Biomedical Imaging virtual special issue "Sub-diffraction Chemical Imaging".

Arianna N. Lacen and Hui-Ting Lee*

Cite This: *Chem. Biomed. Imaging* 2024, 2, 659–682

Read Online

ACCESS | Metrics & More | Article Recommendations

ABSTRACT: Chromatin organization plays a key role in gene regulation throughout the cell cycle. Understanding the dynamics governing the accessibility of chromatin is crucial for insight into mechanisms of gene regulation, DNA replication, and cell division. Extensive research has been done to track chromatin dynamics to explain how cells function and how diseases develop, in the hope of this knowledge leading to future therapeutics utilizing proteins or drugs that modify the accessibility or expression of disease-related genes. Traditional methods for studying the movement of chromatin throughout the cell relied on cross-linking spatially adjacent sections or hybridizing fluorescent probes to chromosomal loci and then constructing dynamic models from the static data collected at different time points. While these traditional methods are fruitful in understanding fundamental aspects of chromatin organization, they are limited by their invasive sample preparation protocols and diffraction-limited microscope resolution. These limitations have been challenged by modern methods based on high- or super-resolution microscopy and specific labeling techniques derived from gene targeting tools. These modern methods are more sensitive and less invasive than traditional methods, therefore allowing researchers to track chromosomal organization, compactness, and even the distance or rate of chromatin domain movement in detail and real time. This review highlights a selection of recently developed methods of chromatin tracking and their applications in fixed and live cells.

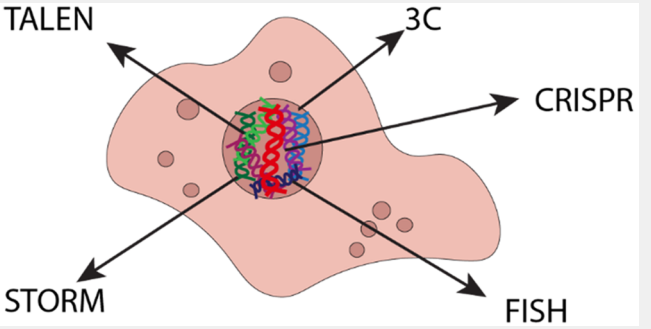

KEYWORDS: *chromatin tracking, chromosome conformation capture, FISH, STORM, telomere, CRISPR, live-cell imaging, centromere, chromatin compaction*

INTRODUCTION

In eukaryotes, DNA in the nucleus is organized into a protein–DNA complex known as chromatin. Chromatin regulation and modification has been implicated to serve as a "signaling hub" for regulation of gene expression, and errors in chromatin packing have been correlated to downstream errors in expression and regulation.[1] The simplest structural unit of chromatin, the nucleosome, is comprised of two copies of each histone (H2A, H2B, H3, and H4) wrapped in approximately 150 base pairs (bp) of dsDNA.[1−3] The formation of nucleosomes gives a minimum chromatin diameter of approximately 10 nm[2]. Nucleosomes were once thought to be static, but recent studies have shown that they are dynamic. Nucleosomal dynamic changes involve differences in chromatin compactness, accessibility, and various complex interactions with other proteins. It has been shown that DNA spontaneously unwraps itself from the histones[4−7] and that this unwrapping is influenced by the ionic conditions of the solvent.[8,9] Furthermore, modifications of the histones themselves have been shown to affect protein–DNA interactions. For example, lysine acetylation at site-specific residues can modulate interactions between the histone and the DNA as well as potentially recruit reader proteins.[10−12]

Once the DNA is coiled around a histone octamer, chromatin can adopt multiple conformations depending on environmental conditions. At physiological conditions, the nucleosomes have an increased propensity for self-interaction. Interactions between nucleosomes are mediated by histones H4 and H2A, which have been shown to lead to nucleosome stacking and the subsequent formation of 30 nm fibers.[13,14] These 30 nm fibers can then be further condensed into larger loops until the chromatin is arranged into fully condensed chromosomes during cell division.[13,14] While evidence for chromatin fibers *in vivo* has been seen in some nuclei in early literature,[13,15,16] visualization of these structures has proved

Received: April 2, 2024
Revised: June 12, 2024
Accepted: June 13, 2024
Published: June 25, 2024

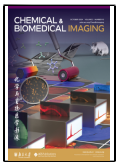

https://doi.org/10.1021/cbmi.4c00033
Chem. Biomed. Imaging 2024, 2, 659–682

Table 1. Overview of Advantages and Disadvantages of Selected Techniques for Chromatin Tracking[a]

technique	advantages	disadvantages	reference
3C-based techniques	• high level of detail	• cannot be used for dynamic information	review: 21; selected works: 22, 25−30
	• high throughput	• resource intensive	
	• versatile	• time-consuming	
FISH and IF-FISH	• low detection limit	• time-consuming	reviews: 31, 35, 36; selected works: 39−41
	• can stain short sequences	• applicable mainly in metaphase	
	• stable fluorescence	• requires high RNA load	
	• versatile		
STORM/pathSTORM	• highly sensitive	• requires cell fixation	reviews: 56, 57; selected works: 63, 65, 68
	• high resolution	• time and resource intensive	
	• can be used with ultrathin (700 nm) sections of tissue		
CRISPR-based techniques	• can label repetitive or nonrepetitive sequences	• can require high sgRNA load	reviews: 100, 101, 164; selected works: 113, 114, 117, 123, 126
	• can be modulated to reduce background fluorescence	• size of complex can potentially disturb natural motion of chromatin	
	• highly modifiable	• requires stable cell lines for endogenous expression of protein	
	• can be multicolor		
	• machinery can be induced or introduced to cell using more mild conditions than FISH, can be used to monitor chromatin in real time		

[a]3C = chromosome conformation capture. FISH/IF-FISH = fluorescence/immunofluorescence *in situ* hybridization. STORM/pathSTORM = stochastic optical reconstruction microscopy/pathological STORM. CRISPR = clustered regularly interspaced palindromic repeats.

difficult due to the small diameter of chromatin and the high density of DNA in the nucleus. The 10−30 nm diameter of the chromatin is beyond the 250−300 nm diffraction limit of commonly used dye and oil immersion objectives. During the interphase, the loosely packed chromatins spread within the nucleus; therefore the chromatin has a low contrast against the rest of the DNA in the nucleus.

Evidence of chromatin fibers has been collected using different methods, such as electron microscopy,[17] scanning force microscopy,[18] and atomic force microscopy.[19] The chromatin undergoes dynamic unpacking and condensation during different phases of the cell cycle. The dynamic environment emphasizes the importance of understanding how chromatin organizes and moves through the cell as the cell cycle turns and its role in genomic organization. With the advent of super-resolution microscopy coupled with computer simulations, it has been shown that chromatin fibers form clusters of heterogeneous nucleosome groups.[20] The association of the nucleosomes in a heterogeneous matter cannot be studied using classical cross-linking methods that impart static information and instead requires methods that can elucidate the organization of higher order chromatin structure. Classical methods of understanding the organization of chromatin relied on either reconstructive methods from cross-linking or fluorescence-based direct visualization. Two of the most popular classical methods of studying higher order structures of chromatin are chromosome conformation capture (3C) and fluorescence *in situ* hybridization (FISH) based techniques. A summary of the advantages and disadvantages of selected classical and newer methods discussed in this review can be found in Table 1.

EARLIER METHODS

Chromosome Conformation Capture (3C)

Chromosome conformation capture (3C) techniques have been used to identify wide-ranging chromosomal contacts (see recent review by Kim and Dekker[21]). Chromosomal contacts, that is, interactions between two or more distal regions either within or between chromosomes, have been implicated in disease, aging progression, and gene regulation and expression.[22,23] For example, changes in the contacts between chromosomes in various cell types have been associated with autism spectrum disorders, obesity, and macrocephaly.[22] The long-ranged nature of chromosomal contacts and their overall stability make them an excellent target for 3C-based techniques. As shown in Figure 1-1, 3C-based techniques rely on cross-linking existing chromosomal contacts through the covalent bonds generated by chemical regents such as formaldehyde (see review by Hoffman et al.[24]). The cross-linked chromatins are then digested with restriction enzymes and ligated. The cross-links are later removed so that DNA sequences in close proximity can be sequenced and reconstructed. The contacts can then be turned into molecular models that can be validated with other techniques such as DNA-FISH, RNA-seq, and ChIP-seq, as well as computer simulations, to connect chromatin contacts with gene expression. In studying chromosomal folding, for example, 3C was used to show that the third chromosome of yeast (*Saccharomyces cerevisiae*) was a 3D contorted ring.[25] However, because 3C involves PCR to detect ligated fragments and thus requires specific primers, it requires prior knowledge of existing contacts.

To overcome the limitation of 3C, methods based on 3C were developed to use a universal primer for all the fragments. For example, 5C, or chromosome conformation capture

https://doi.org/10.1021/cbmi.4c00033
Chem. Biomed. Imaging 2024, 2, 659−682

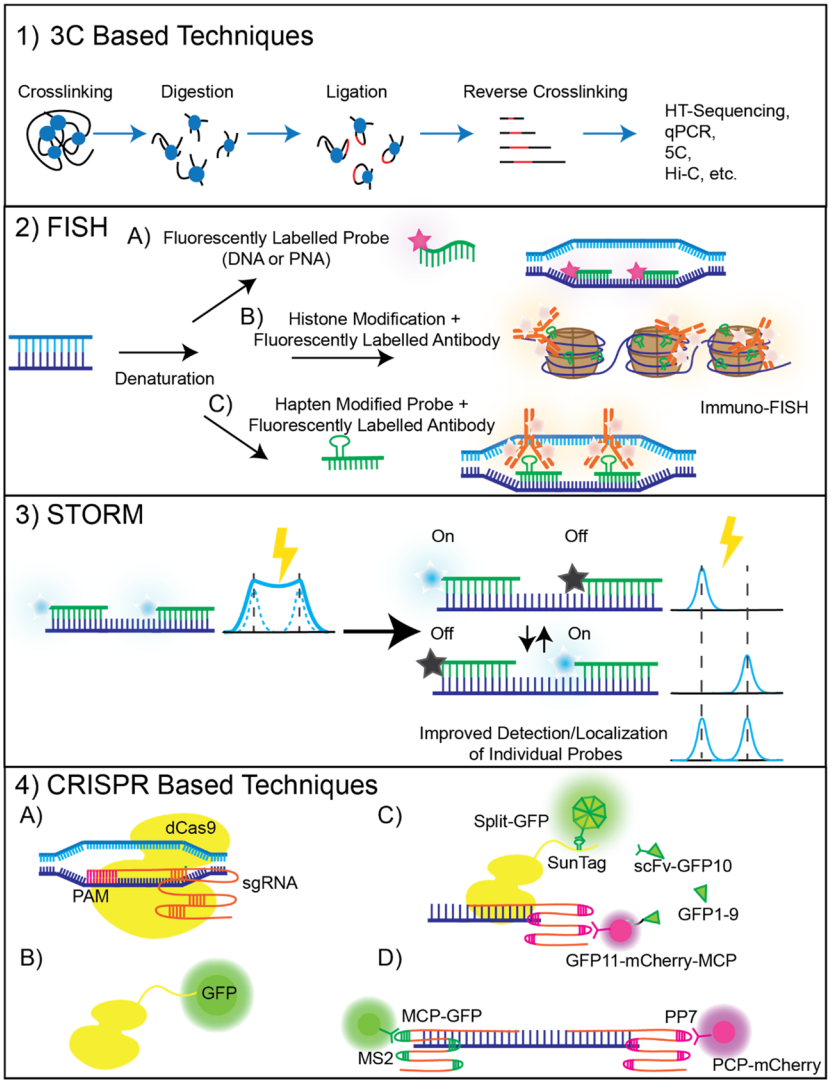

Figure 1. Overview of selected chromatin tracking techniques showing general features of each technique. (1) 3C-based techniques focus on cross-linking chromosomal contacts, digesting chromatin, and ligating the resulting chromatin fragments. The cross-links are then reversed, and then sequencing is performed on the chromatin fragments, which can be done in a variety of ways. (2) FISH and immuno-FISH rely on local denaturation of chromatin target and then hybridization of various moieties that are either fluorescently labeled or recruit fluorescently labeled antibodies. (3) STORM relies on the blinking of dyes and their localization to reconstruct the structure of the genomic target at a super-resolution. (4) The CRISPR system requires Cas9, sgRNA, and a PAM motif (A). CRISPR-based imaging techniques invariably require some component of the system to be fluorescent, whether it is the dCas9 (B), a split fluorophore (C), or fluorescent proteins specific to a motif on the sgRNA (D).

carbon copy, utilizes universal primers that are ligated to all sequence fragments over typically no more than a megabase (Mb).[26] 5C was used to provide evidence for topological-associated domains (TADs) and has also been used to study X-chromosome inactivation in mice.[27] 5C can interrogate over 250 000 possible chromosomal contacts in parallel with a mean resolution of 10−20 kb.[27] Another particularly popular variant of 3C is Hi-C, which uses universal primers and high throughput sequencing to reveal all possible pairs of sequence fragments. The workflow of Hi-C requires the cross-linking and digestion of DNA as done in 3C. The main difference in Hi-C comes in the generation of a 5′ overhang from the digestion product.[28] To this overhang biotinylated oligonucleotides are annealed and ligated to produce blunt ended DNA. Once biotinylated, the sequences can be selected via streptavidin−biotin binding and used to create a library for next-generation sequencing. Once the DNA has been sequenced, a model of the chromosome can be reconstructed to evaluate the structure. Because each DNA fragment is individually aligned to the genome, Hi-C can detect all possible chromosomal contacts. The resulting contact maps of reconstructed chromosomes show that the same regions across chromosomes were either along the surface of the chromosome or buried within the chromosome.

Hi-C was integral to our understanding of which regions of chromatin were expression-active (A) or expression-inactive (B), dividing chromatins into so-called A/B compartments.[28,29] This technique has also revealed that the general topology of the genome is conserved across cells, that is, A or B compartments always stay together and that the A compartment is always separate from the B compartment. The disappearance of A and B compartments has been noted during anaphase and telophase; however, the component genes located in each compartment do not switch between compartments.[30] Hi-C has also revealed how complex the orientation of chromatin is inside the nucleolus, with an outer

https://doi.org/10.1021/cbmi.4c00033
Chem. Biomed. Imaging 2024, 2, 659−682

B ring, an inner A ring, and an internal B region that surrounds a hollow nucleolus. Hi-C also allows for the understanding of complex fold formation, with "snapshots" taken at various time intervals via arresting cells at various stages in the cell cycle.[30] Overall, 3C-based techniques provide a high level of detailed structural information on chromosomal conformation, identify conserved regions of expression, and identify potential disease targets. However, despite its pros, 3C techniques retain a few important limitations. As every 3C variation relies on fixation of the DNA using cross-linking, 3C and related techniques can only be used to get static information, and thus dynamic information can only be inferred. In addition, these techniques are resource- and time-intensive, with preparation and execution lasting several days. Perhaps most importantly, 3C-based techniques can be limited over the range of chromatin to be analyzed and often rely on preestablished knowledge of at least some of the contacts within a given structure, requiring precise primer design.

Immunofluorescence (IF) and Fluorescence *In Situ* Hybridization (FISH)

Fluorescence *in situ* hybridization (FISH) and immunofluorescence (IF) are methods of structure determination that do not rely on digestion of chromatin but use hybridization or binding of fluorescent probes to the targeted genomic locus. In contrast to 3C-based methods, FISH does not require fixation and DNA digestion and therefore leaves the target DNA relatively intact.[31,32] However, it should be noted that FISH does require local DNA denaturation to allow hybridization of the probe. The most popular method of DNA denaturation is heating the sample to 65−70 °C, and a chemical fixation step is often added to the heat denaturation to preserve the structure (see a standard protocol from Young et al.[33]). FISH has been used extensively to track genomic targets using fluorescently labeled probes, typically consisting of either DNA or peptide nucleic acid (PNA). FISH probes are complementary to the genomic target of interest and hybridize to the target sequence once transfected into the cell or during heat denaturation of the genomic DNA[32,34] (see Figure 1-2A). IF of chromatin uses antibodies that recognize chromatin proteins, typically histone proteins or other heterochromatin markers, to achieve immunostaining of the chromatin locus[15,35] (Figure 1-2B). Antibodies can also be designed to bind to backbone modified oligonucleotide probes, such as hapten-modified probes (Figure 1-2C). The primary antibody can either be directly labeled with fluorophores or recognized by a fluorescently labeled secondary antibody.[35] Once hybridized or bound to the target sequence or protein, the fluorescence of the probe or antibody can be detected using various microscopy techniques, most commonly wide-field or confocal microscopy, and notably the recently developed STORM (stochastic optical reconstruction microscopy; see Recent Methods for Improving Imaging Resolution). FISH and IF allow for the determination of how target DNA localizes to different parts of the cell. FISH and IF can also be used to track the colocalization of multiple genomic targets and in this way can be used to extract distance information between a pair of genomic loci. By measuring the distance between two or more FISH or IF signals, changes in chromatin length or compactness can be monitored. However, due to the low fluorescent intensity of individual probes under most diffraction-limited fluorescent microscopes, FISH relies on redundant sequences to allow for hybridization of multiple probes to increase signal intensity. Therefore, highly repetitive regions of the chromatin were the major targets of chromatin structural study using FISH, and multiple fluorophore-carrying antibodies are preferred in IF.

FISH's suitability for labeling redundant sequences makes it ideal for studying the telomeric region of the chromosome. The telomeres of mammalian organisms are comprised of 10−15 kb of TTAGGG repeats with a 3′ single-stranded overhang that is between 50 and 300 nucleotides long.[36,37] Telomere length has long been shown to vary depending on the cell type, age of the cell, and various other factors.[36−38] The heterogeneous length of telomeres and their attrition have been correlated to cells entering senescence; thus monitoring the length of telomeres throughout the cell cycle presents a promising area of study that FISH is well-suited for. To this end, work has been done to relate telomere length quantification to gender, age, and even cognitive impairment.[39] Work by Canela et al.[39] reports a rate of telomere attrition of 71−72 bp/year using high-throughput quantitative FISH (HT Q-FISH) on peripheral blood lymphocytes. Interestingly, their work revealed a geographic discrepancy wherein French subjects had a slower rate of telomere attrition (54 bp/year) than age-matched Italian subjects (60 bp/year), possibly suggesting a combination of environmental and genetic factors in influencing telomeric length. Other studies have used FISH to suggest that endogenous telomerase is necessary for maintaining critically short telomeres.[40] Röth et al.[40] blocked endogenous telomerase expression in human T cells and saw a decreased lifespan along with cytogenetic abnormalities, including chromosomes completely lacking telomeric regions. More recently, FISH was used to monitor alternative lengthening of telomeres (ALT) in the homology-directed synthesis of telomeres.[41] This group found that, using FISH, they could monitor double-stranded DNA break (DSB) responses in ALT positive and negative cells. TRF1-Fok1 expression induced kilobase long DSBs that extended into the subtelomeric region which resulted, surprisingly, in 4-fold increases in average telomere foci size in ALT positive cell lines that did not have active telomerase. The DSB responses lead to increasing numbers of subtelomeric FISH signals to cluster at what would be a telomere, indicating that DSB responses provide a stimulus for telomere clustering. Indeed, this movement and clustering were tracked by chromosome-orientation FISH (CO-FISH) to interrogate telomere chromatid exchanges and revealed that the forces driving telomere movement were connected to ALT telomere recombination.

The denaturation step in the popular FISH protocol may impact or destroy the DNA double helix and cause artifacts due to interactions between the DNA and the denaturing agent, which are typically chaotropic.[42] The disruption to the local secondary structure can be minimized by various methods including RASER-FISH, which uses local exonuclease digestion to allow for direct hybridization of the FISH probe to the target locus;[43] FISH conducted at low temperature;[44] and GOLD-FISH, which uses helicase activity at specific genomic loci to unwind DNA allowing for hybridization of the probe.[45] These methods, particularly low temperature FISH and GOLD-FISH, do not have the harsh denaturation step and largely leave the DNA intact. In low temperature FISH, hybridization of the DNA probe takes place entirely at 37 °C over a long period of time to ensure optimal hybridization of the probe to the target DNA.[44] In this way, the gentler conditions mean that cells would not have to be fixed.

https://doi.org/10.1021/cbmi.4c00033
Chem. Biomed. Imaging 2024, 2, 659−682

To eliminate the need for DNA denaturation, triplex forming oligonucleotides (TFOs) or polyamides have been used as tools for gene targeting and more recently chromatin tracking.[46,47] TFOs are short (under 30 nt) nucleic acids that are designed to be major groove binders of A-form or B-form dsDNA, preferentially in oligopurine or oligopyrimidine tracts.[48] While canonical dsDNA is held together through Watson−Crick base pairing, TFOs bind to the duplex through Hoogsteen base pairing between the pyrimidine bases on the TFO and the oligopurine tract in the target gene. Under neutral pH (pH 7), only thymines in the TFO can form Hoogsteen pairs with the adenine in the target.[49] However, in acidic conditions, protonation of cytosine on the TFO allows the cytosine to form Hoogsteen pairs with guanines in the target.[50,51] The special requirement of oligopurine tracts means TFO can only be used to track targets with this specific pattern, which require special consideration for the target selection.[52] TFOs and FISH have shared principles of hybridizing nucleic acids to a genomic target and their ability to be fluorescently labeled. However, FISH techniques require local denaturation as the probes compete with the genomic sequence for the complementary strand, which can affect local chromatin dynamics. Using TFOs eliminates the denaturation requirement as they do not replace one strand in the dsDNA; therefore, it is proposed to be a less disrupting method for live-cell imaging. However, introduction of TFOs into cells can still be challenging.[46] The most common TFOs are PNAs (see above) which have commonly been used for tracking chromatin dynamics.[53]

Quick Summary of Earlier Methods

Earlier methods have been used to accomplish fundamental understandings of chromosome structure and organization, as well as to provide a basis for tracking chromatin localization. These techniques are now most commonly used in conjunction with or to validate newer methods. While these standard techniques have, on their own, contributed much to our understanding of chromatin dynamics, regulation, and organization, much is left to be solved on how chromatin can be more effectively labeled, studied, and utilized. Most earlier fluorescent-based imaging methods have relied on usage with wide-field and confocal microscopies, which have limited resolution due to the diffraction limit.[54,55] The more recent methods overcome this limitation by using super-resolution microscopy and newer labeling methods that are applicable for diffraction-limited microscopes, as detailed in the next sections.

RECENT METHODS FOR IMPROVING IMAGING RESOLUTION

STORM and STORM Derivatives

The main challenge left by Hi-C and traditional fluorescent microscopy methods (FISH and IF) is the lack of description of chromatin physical structure in a cell at the resolution of the kilobase (kb) to megabase (Mb) scale. STochastic Optical Reconstruction Microscopy (STORM) has emerged in recent years as the new standard in super-resolution microscopy.[56−59] With a spatial resolution of 20−50 nm, STORM offers a level of detail 10-fold higher than traditional fluorescent microscopy while still employing the relatively simple setup and sample preparation of FISH and IF.[57,60] STORM relies on the random blinking of photoswitchable fluorophores. The fluorescent signal of each fluorophore in individual images within the full movie is used to calculate the spatial coordinate of the fluorophore; then the spatial coordinates of all the fluorophores are used to reconstruct the shape or traces of the targeted structure or molecule (see Figure 1-3). The applications of STORM and its derivatives range from imaging of individual microtubules to tracking to colocalization of histone proteins to identifying the effects of differing gene regulation.[56,58,61] The major drawbacks of STORM come from the requirements of specific photoswitchable fluorophore and imaging buffers that are toxic to cells. Also, as each reconstructed STORM image is comprised of a long movie with hundreds of thousands of individual high-resolution images or more, this method can easily create large volumes of data.[56]

Oligopaint and Multiplexing STORM. STORM is most typically used in conjunction with FISH to track chromatin in cultured cells because STORM can resolve the fluorescent signal of probes beyond the diffraction limit. The high resolution means that subtle rearrangements of chromatin organization can be more closely followed. However, like the conventional diffraction-limited FISH, STORM requires multiple fluorescent dyes to locate at the same locus of interest because STORM relies on the random blinking of multiple dye molecules. To satisfy the multidye requirement and to allow imaging of nontandem repeat regions of the genome, special designs of FISH probes have been developed to label a long tread of nonrepetitive sequences with the same dye. The simplest approach is to create a pool of FISH probes that each bind to a unique sequence of the target gene and all carry the same type of fluorescent dye. A more advanced approach, named Oligopaint, uses two sets of oligonucleotide probes, primary and secondary, to allow multiple dye molecules to localize at the same gene and complex reconstruction of different sections with different sets of dyes. In general, the primary probes contain genomic and nongenomic sequences. Each probe in a set of primary probe "pool" contains a unique sequence in the genomic part, which is complementary to a unique, nonrepetitive part of the target gene. Primary probes in the same pool contain the same nongenomic sequence which binds to the labeled secondary probes. Each of the primary probes may contain one or more shared nongenomic sequences, to allow the binding of one or more secondary probes.[62−64] With the two-probe set design, Oligopaint allows multicolor labeling of the same or different genomic loci. The secondary probes of Oligopaint can be hybridized to the sample sequentially, as the dye in the first secondary probe is photobleached before the next secondary probe is introduced. This approach allows different parts of the same or different target gene to be differentiated and decoded, which gives the multiplexing capability of FISH-based STORM.

Bintu et al.[65] combined the multiplexing capability of FISH with STORM to track the rearrangement of chromatin at the TAD and subTAD levels. Multiplexing using FISH involves using nonfluorescent primary probes to anneal to the target sequence and then introducing fluorescent readout probes (secondary probes) that anneal to the primary probes. The readout probes are imaged and then quenched between rounds of hybridization to identify different regions of target sequence.[66] Using 12 000−25 000 primary probes, they were able to label several Mb of human chromosome 21 into consecutive 30 kb segments. Each probe was hybridized to 20 nucleotides (nt) of target sequence within each 30 kb fragment to facilitate multiplexed FISH. After hybridization of the primary probes to the target sequence, dye-labeled readout

https://doi.org/10.1021/cbmi.4c00033
Chem. Biomed. Imaging 2024, 2, 659−682

probes are hybridized to the primary probes. The dye-labeled probes are then imaged through STORM. After imaging, the dye-labeled probes are either extinguished or removed, and another readout probe is introduced to hybridize to the primary probes of the next 30 kb fragment. This process is continued until all several Mb of the target sequence are imaged. The STORM image readout can then be used to reconstruct a super-resolution image of the target sequence with several pseudocolors, with each pseudocolor corresponding to a unique 30 kb fragment, as seen in Figure 2A.

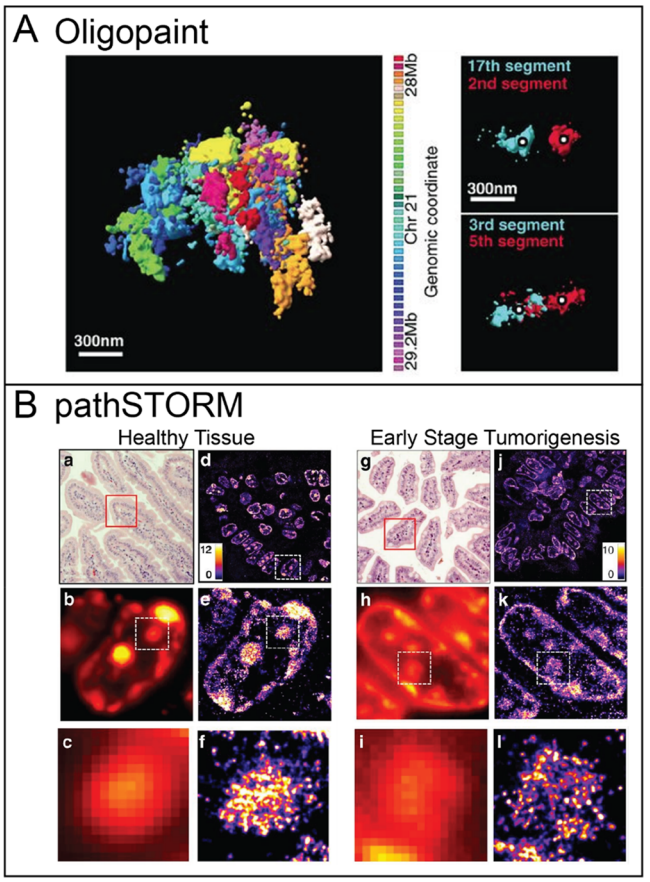

Figure 2. Oligopaint and pathSTORM. (A) Reconstructed 3D STORM images obtained through Oligopaint of 41 consecutive 30 kb chromatin segments in a 1.2 Mb region of chromosome 21 (Chr21:28Mb−29.2Mb), each represented in pseudocolors. Reprinted in part with permission from ref 65. Copyright 2018 Bintu et al. (B) (a, g) H&E-stained pathology images and (d, j) pathSTORM images of H3K9me3-bound heterochromatin in healthy (right) and early stage tumorigenesis (left) tissue in 6 week ApcMin/+ mice. Scale bar, 10 μm. (b, h) Wide-field fluorescence images and (e, k) corresponding pathSTORM images of heterochromatin from a single nucleus. (c, i) and (f, l) Zoom-in regions of (b, h) and (e, k). Reprinted in part with permission from ref 68. Copyright 2020 Xu et al.

Combining FISH and STORM in this way results in conformation maps with less than 50 nm error in probe localization and less than 5% error in physical size when validated against established methods such as Hi-C (see earlier).

Bintu et al. utilized the multiplex FISH and STORM approach to study the arrangement of chromosomal interactions into TAD-like structures. Whereas other methods of studying TADs have suggested that TAD-involved regions of chromatin are conserved between cells, this group noted that chromatin regions involved in TADs varied between cells. Using STORM, they were able to quantify the boundaries of these TAD-like regions and noted substantial differences in domain boundaries between individual cells and an overall preference to form at positions known to be bound by CCCTC-binding factor (CTCF) and cohesin. CTCF and cohesin are known to regulate the 3D structure of chromatin by binding DNA strands together and anchoring the chromatin to cellular structures such as the nuclear lamina.[67] Interestingly, the authors note the resilience of TAD-like structures even in cohesin depleted cells.

The combination of FISH and STORM was also used to study known TADs within chromosome 21 across various stages of the cell cycle. While the variations in TAD domain boundaries were negligible between G1, S, and G2 phases, there were moderate changes in the strength of TAD organization, suggesting that the transition from G1 to G2 may weaken TADs.

pathSTORM. While most STORM studies are conducted with a single layer of cells, a particular derivative of STORM, pathSTORM, has been utilized to visualize higher order chromatin structure in fixed pathological tissue, hence the name. pathSTORM, for pathological STORM, obtains high-quality super-resolution images of chromatin by reducing the background, increasing the selectivity of fluorophore emittance to further lower the background, and improving localization methods for overlapping fluorophores in pathological tissue.[68] In normal STORM, it becomes difficult to adequately reconstruct the target locus in cell tissue due to buildup of signal.[56] pathSTORM takes several considerations to limit background fluorescence while still being able to image the target locus throughout the tissue sample, largely due to sparse distribution of single fluorophores with nanometer precision. Although it still requires sample fixation and FISH or IF prior to imaging, pathSTORM has the added benefit of being able to image ultrathin (700 nm) sections of tissue instead of single-layer cultured cells. pathSTORM of tissue sections has been used to detect disrupted higher order folding in early carcinogenesis in mice that undergo intestinal tumorigenesis. While IF staining the chromatin with Alexa Fluor 647-conjugated secondary antibodies to visualize various histone markers associated with heterochromatin in intestinal epithelial cell nuclei, conventional wide-field fluorescence images showed large, dense regions of heterochromatin in all tissue types tested. The super-resolution images revealed that these dense regions are the result of nucleosome nanoclusters as seen in Figure 2B. These nanoclusters were determined to be large and clustered in wild-type healthy mice but smaller and further apart in early stage tumorigenic mice. In later stages of cancer, the observed structural changes became more pronounced, displaying fragmentation of heterochromatin clusters and the loss of higher order compaction. This loss of compaction may indicate that disruption of higher order structure is necessary for malignancy of precursor lesions.

pathSTORM shows that the change in chromatin nanoclusters is not limited to intestinal tumorigenesis. Such clusters have also been seen in human fibroblast nuclei (hFb). In the reports by Ricci et al.,[20] cells were arrested in the interphase between G1 and S to observe the clustering of H3 and H2B, two key components of the nucleosome, in order to visualize the compactness of chromatin. Treating cells with Trichostatin

https://doi.org/10.1021/cbmi.4c00033
Chem. Biomed. Imaging 2024, 2, 659−682

A, an inhibitor of histone deacetylase enzyme, has been shown to lead to decondensation of chromatin through changes in the binding capacity of the histones to DNA.[69] Tracking the density of the chromatin nanoclusters through changes in the signals of H3 and H2B revealed dimmer spots that were more dispersed in the nucleus. Thus, after treatment with Trichostatin A, hFb exhibited the expected loss in chromatin compactness. Going further, tracking chromatin in pluripotent stem cells through STORM reveals that more chromatin clusters correlate with lower pluripotency.[20] It could thus be argued that higher levels of chromatin structure limit the accessibility of DNA that would be necessary for various differentiation routes for the stem cell. In general, FISH- or IF-based STORM provides super-resolution images that can resolve subtle changes in chromatin organization that traditional fluorescent microscopy cannot. However, the sample fixation and long image acquisition time of STORM make live-cell chromatin tracing with STORM challenging.

PALM

Similar to STORM, PhotoActivated Localization Microscopy, or PALM, has proven to be a versatile super-resolution imaging technique. With a similar resolution to STORM, PALM has been used to visualize cellular structures in biological samples within a few nanometers. PALM is notable for its use of photoactivatable fluorescent proteins, such as photoactivatable green fluorescent protein (PA-GFP). These fluorescent proteins can be expressed endogenously, thus making PALM suitable for live-cell imaging as no denaturation step is necessary.[70] However, whereas STORM relies on the blinking of fluorescent molecules, PALM instead confines the life of the fluorophore within a limited time interval and requires continuous emission of light from the fluorophore, until it eventually photobleaches. In this way, subsets of the sample are illuminated, which allows for localizing the fluorophore with high precision. The main advantage of PALM over STORM is that PALM can use fluorescent proteins that are expressed in the cell. Therefore, super-resolution live-cell imaging has become possible. PALM has been used in a number of applications from tracking the organization of focal adhesions in live cells[71] and chemotaxis networks in *E. coli*[72] to quantitatively tracking individual fluorophores.[73,74]

Deep Learning Based Super-Resolution Imaging

Both STORM and PALM belong to the family of single-molecule localization microscopy, which reconstructs the coordinate of an individual molecule from its emission signal in different frames of microscope movies. The coordinate reconstruction process requires heavy computational calculation, which is time and energy consuming and can be prone to artifacts if calculation parameters are not properly evaluated (see recent review by Liu et al.[75]). Multiple research groups have been working on improving the localization of fluorophores and thus the precision of the reconstructed images. One such development utilizes deep learning to predict super-resolution images from fluorescence emitters, such as DeepSTORM[76] and Deep-PALM.[77] In Deep-PALM of live-cell chromatin imaging, the locations of fluorophores in the next time point or frame are predicted using a convolutional neural network (CNN) trained on labeling densities. It is noteworthy that the labeling density of the fluorophore has a direct effect on the specificity of CNN analysis. Too high of a labeling density lowers the localization specificity, while too low of a labeling density does not allow for accurate reconstruction of the target locus. Due to the predictive nature of Deep-PALM, it improves live-cell-imaging outcomes because an accurate representation of structural motion can be constructed from fewer emitters over a shorter excitation period, which lowers the chance of inducing phototoxicity in the cells as well as lowering the need for high protein expression. However, because the reconstructed image is a summation of the individual predictions, there is a trade-off between prolonged acquisition time and motion blur.[71] Barth et al. were able to find a balance between emitter sampling and motion blur buildup at a time resolution of 360 ms, allowing for more data collection while retaining the resolution of data.[77] Imaging histone protein H2B fused to photoactivable red fluorescent protein (PA-tagRFP) in live cells revealed a clear nuclear periphery with variable density in the nuclear interior that varied over the imaging time span, shown in Figure 5A. Changes in the density of chromatin observed with Deep-PALM corroborate observations of chromatin density seen with other techniques discussed in this review.[20,61,78] Even at the periphery, conformational changes were observed for approximately 1 s, with a spatial resolution of 63 ± 2 nm.

Notably, Deep-PALM has been used to identify the dynamics of chromatin "blobs" or clustered nucleosomes as they shift in shape over approximately 1 s.[79] Each blob is thought to consist of less than 30 nucleosomes that transiently interact with each other and may have as of yet unknown function. Using Deep-PALM, researchers sought to determine whether chromatin dynamics within a chromatin blob influences the organization of said blobs using Granger causality. Granger causality determines whether one variable as part of a time series can be used to predict another.[80] Determining the Granger causality of the chromatin dynamics using Deep-PALM revealed that chromatin dynamics (described as the instantaneous flow or velocity of a blob) is a key determinant of nanoscale chromatin organization in terms of nearest neighbor distance and blob area. Nearest neighbor distance refers to the distance from a defined point (in this case a specific chromatin blob) to its nearest neighboring point (in this case the next closest chromatin blob).[81] Fluctuations in the chromatin dynamics change the nearest neighbor distance; thus it can be inferred that blob creation and condensation are actively driven processes rather than a randomly diffusive process. Overall, Deep-PALM represents a powerful technique for coupling chromatin structure and organization with their dynamics, but it is limited by the labeling density of the fluorescent proteins used.

Fluorescence Lifetime Imaging Microscopy–Förster Resonance Energy Transfer (FLIM–FRET)

Fluorescence lifetime imaging microscopy (FLIM) has emerged as a sophisticated method of tracking a fluorescently modified substrate by tracking the fluorescence lifetime of the fluorophore. Typically, the lifetime of the fluorophore is on the order of pico- to nanoseconds and retains a high sensitivity to not only its environment but also to the state of the molecule it is bound to (see review by Datta et al.[82]). Depending on the fluorophore, FLIM can be used in conjunction with another highly sensitive imaging technique known as Förster resonance energy transfer (FRET). In FRET, two fluorophores are used that can transfer energy from a donor fluorophore to an acceptor fluorophore. The distance between the two determines the degree of energy transfer, where the closer the two fluorophores are the greater the energy transfer and

https://doi.org/10.1021/cbmi.4c00033
Chem. Biomed. Imaging 2024, 2, 659−682

thus the greater the fluorescence intensity of the acceptor.[83−85] When FRET occurs, the fluorescent lifetime of the donor will also be reduced because the energy is transferred to the acceptor. Depending on the FRET dye pair used, the sensitivity of the distance measurement provides nanometer resolution.[85,86] Combining the two techniques gives FLIM−FRET, where first the donor fluorophore is excited by laser light and the lifetime of the donor is measured by FLIM, and if the donor comes close (1−10 nm) to the acceptor fluorophore while being excited, the acceptor starts to fluoresce, and is quantified.

FLIM−FRET has been applied to numerous biological systems owing to its relative simplicity and high specificity of signal (see refs 82 and 87). For example, FLIM−FRET has been used to monitor changes in chromatin compaction in *Caenorhabditis elegans in vivo* at the nanoscale.[88] Germline *C. elegans* was grown that stably expressed GFP-H2B and mCherry-H2B fusion proteins, referred to as the 2FPs-H2B strain. The fluorescent protein attachment sites used in this system set the two fluorescent proteins far apart, so no FRET could occur if both GFP-H2B and mCherry-H2B were incorporated in a single nucleosome. FLIM was measured and revealed that the fluorescence lifetime (τ) of 2FPs-H2B was lower (2.3 ns) than that of germline *C. elegans* only expressing GFP-H2B (τ = 2.6 ns), as shown in Figure 4D1,D2. This decrease can be attributed to FRET from GFP to mCherry when the sample is illuminated under GFP excitation. Monitoring the FRET signal in pachytene stage cells (the stage with highly structured chromatin in preparation for crossing over, recombination, etc.),[89] FLIM−FRET revealed four different classes of energy transfer: sublow, low, intermediate, and high FRET as shown in Figure 4D3. These classes can be translated into heat maps that demonstrate the differing levels of chromatin compaction. The heat maps show that, even in highly structured chromatin, compaction at the nanoscale is heterogeneous. It could be assumed based on the FRET principle that high levels of FRET would lead to low levels of FLIM, but what was seen is that, while regions of high FRET/low FLIM exist, there are significant areas of intermediate and low FRET that correspond to low FLIM. Plotting the GFP-H2B intensity and GFP-H2B lifetime in 2FPs-H2B cells gave a negative linear relationship (r = −0.263) between the two. This may suggest that the decrease in GFP-H2B lifetime is not solely due to FRET with mCherry and might be related to the local chromatin environment affecting the fluorescence lifetime. Thus, FRET signals of pachytene stage cells reflect not only clustered chromatin but also the local packing state of chromatin. FLIM−FRET can also be used to study the effects of depleting various factors involved in activating or deactivating chromatin on compaction. Silencing certain PTM histones and condensin proteins changes the distribution of observed FRET, which may reflect changes in chromatin morphology. Because of its sensitivity and precision, FLIM−FRET provides a reliable method to study nanometer changes in chromatin compaction. However, for usage *in vivo*, it is important to note that achieving high enough levels of stable fluorophore expression can be challenging and is, at present, best suited for small, transparent model organisms, such as *C. elegans*. Dissection of tissue for imaging provides clearer FRET images, at the obvious expense of losing dynamic information. Going forward, generation of more stable fluorophores and better expression systems may serve to alleviate present concerns of signal intensity.

SIM

Structured illumination microscopy (SIM) has emerged as perhaps the most easily implemented method for super-resolution imaging due to its applicability of use with biological samples already prepared for conventional fluorescence imaging. Whereas STORM and PALM require fluorophores that can go through dark and fluorescent states (blinking or photobleaching) during the experiment, SIM prefers fluorophores to be resistant to photobleaching during image recording.[90] The "structured illumination" in the name refers to the use of patterned illumination, which was originally used to probe surface features.[90,91] When patterns are multiplicative superimposed, moiré patterns or moiré fringes are produced. Analyzing the moiré patterns generated by different illumination patterns at the same sample allows reconstruction of the sample pattern, which is the distribution of desired targets. This technique primarily focuses on improving the lateral and axial resolutions of fluorescence microscopy. To create high-resolution images with SIM, the sample is imaged using different illumination phases of the excitation light until the whole sample is illuminated with all phases. The signals collected at each illumination phase are then analyzed to extract the Fourier components that are used to reconstruct a high-resolution image; see the review by Heintzmann and Huser.[92]

There are multiple ways to structurally illuminate a sample, and each has its own advantages and disadvantages. SIM is capable of operating in either a 2D or 3D functionality. In 2D-SIM, the most common methods utilize two beams of excitation light that produce different fields of illumination. One version, TIRF-SIM, utilizes an evanescent field of light or standing light pattern generated by interfering two laser beams at an angle beyond that of total internal reflection. This method can generate multiple images with unique illumination patterns that can be used to reconstruct the sample image at high resolution.[93,94] However, the illumination area generated this way is shallow, generally no more than 200 nm deep from the total internal reflection interface while using commonly visible light sources. This can limit applicability toward imaging a deeper cellular structure. Another version of 2D-SIM, two-beam SIM, circumvents the shallow illumination area issue by interfering two beams below the total internal reflection angle. This widens the possible viewing area, at the cost of increasing background noise and reduced spatial resolution. Three-beam SIM, or 3D-SIM, retains the two beams mentioned previously but adds a third, central beam to create a 3D excitation pattern. The third beam is typically circularly polarized light, to ensure similar contrast ratios between its vertical light and the other two beams' horizontal light.

Regardless of illumination mode, SIM does not require special labeling of the target nor beyond moderate photostability or blinking. This thus lends the technique to a wide range of biological specimen imaging. One example of such an application is studying mesoscale chromatin organization in fixed and live somatic cells. Miron et al.[95] used 3D-SIM to acquire multicolor super-resolution images of whole cells that showed chain-like structures of chromatin with distinct "links" in the chain of chromatin domains of variable diameter. Previous studies have shown that DAPI-stained chromatin in cell nuclei exists as a spongy mass of chromatin adjacent to chromatin sparse areas that lead into nuclear pores.[96−98] Miron et al. used 3D-SIM in live cells to confirm that the chromatin

https://doi.org/10.1021/cbmi.4c00033
Chem. Biomed. Imaging 2024, 2, 659−682

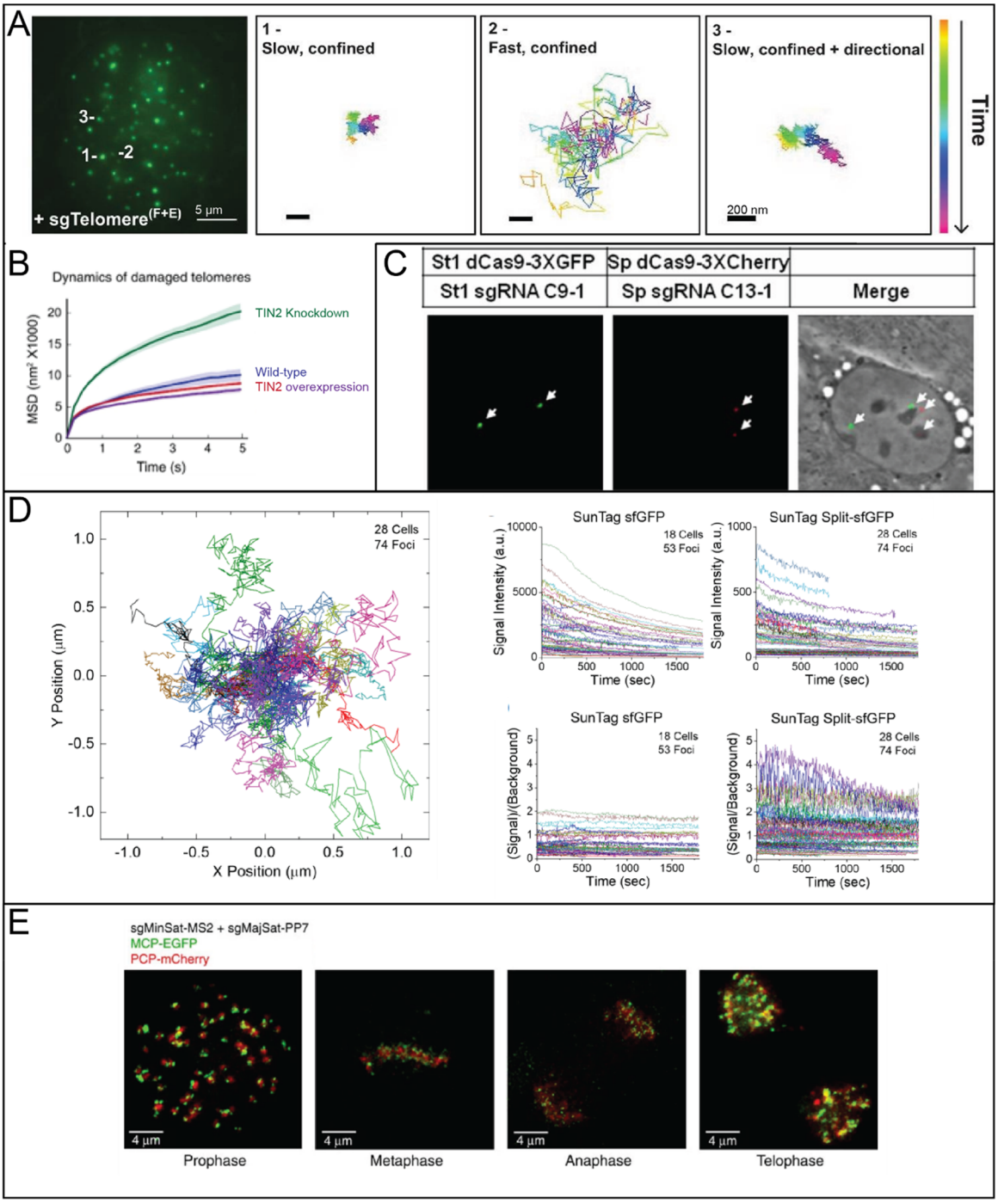

Figure 3. CRISPR Techniques. (A) CRISPR imaging of telomeres and trajectories of three telomeres with different movement modes. The trajectory lengths are 600 frames for 1 and 3 and 260 frames for 2. (B) Averaged MSD curves of CRISPR-labeled telomeres with scrambled shRNA (blue), TIN2 shRNA (green), or coexpression of TIN2 shRNA with the long (red) or short (purple) isoform of TIN2. (A and B) Reproduced in part with permission from ref 111. Copyright 2013 Elsevier Inc. (C) dCas9-3xGFP and dCas9-3XCherry coexpressed with their cognate sgRNAs (sgRNA C9-1 and sgRNA C13-1) to specifically label either pericentromeric sequence in chromosome 9 (left) or repeat sequence unique to chromosome 13 (middle). Right image is merged from left, middle, and phase-contrast images of whole nucleus. Reproduced in part with permission from ref 113. Copyright 2015 Ma et al. (D) (left) Collected trajectories of C9-1 foci (n = 74). All trajectories start at the origin. (right, top row) Signal intensity of C9-1 foci (n = 74) using SunTag Split-sfGFP compared with SunTag sfGFP (n = 53). (right, bottom row) Signal/background ratio of C9-1 foci for the SunTag split-sfGFP and SunTag sfGFP systems. Reproduced in part with permission from ref 117. Copyright 2020 Chaudhary et al. (E) 3T3 fibroblasts expressing dCas9, PCP-mCherry, and MCP-EGFP were transfected with sgMajSat-PP7 and sgMinSat-MS2 to track murine major and minor satellite regions through the cell cycle using time-lapse live imaging. Reproduced in part with permission from ref 114. Copyright 2016 Fu et al.

chains were separated from each other by an interchromatin compartment (IC) but that these features exhibited dynamic behavior over various observation periods. It was found that the movements of these features were coherent, that is, moving in the same direction, consistent with earlier reports on the behaviors of chromatin "blobs" (see earlier and Bruinsma et

https://doi.org/10.1021/cbmi.4c00033
Chem. Biomed. Imaging 2024, 2, 659−682

al.[99]). The nature of the chromatin-free ICs was further explored using 3D-SIM to reveal that the bulk of the ICs were filled with RNA transcripts in mutually exclusive volumes; there was no observed area where RNA and chromatin were observed intermingling. The RNA inhabited an area approximately 200−300 nm in diameter, similar to the size of the chromatin domains. The remainder of the IC volume was found to be most likely a combination of ribonucleoproteins or spliceosomes, albeit in smaller clusters, typically 10−20 nm.

Three-beam SIM was also used to create multicolor images which were then analyzed using machine learning. Based on signal intensity, the fluorescence signal can be translated into a heat map where the coolest colors are chromatin depleted (such as the IC) and hotter colors represent areas of pronounced chromatin density. The chromatin density information is then combined with the signals from known markers for effectors of specific genome functions, which can give the localization of each effector to various regions of chromatin density. For example, RNA polymerase II was enriched in the low chromatin density IC, whereas post-transcriptionally modified (PTM) histones, such as H3K4me3 and H3K36me3, were found to be enriched in moderately dense chromatin areas. These proteins are known to associate with transcriptionally active chromatin, which may explain their proximity to the IC, previously shown to be enriched in RNA transcripts and sparse elsewhere. Conversely, PTM histones associated with transcription repression such as H3K27me3 and K3K9me3 were found to be enriched in chromatin dense areas almost exclusively. The authors note that the differential enrichment of associated chromatin factors may be related to the size of the protein complexes responsible for their localization. Smaller complexes such as those for H3K27me3 and K3K9me3 were found in chromatin dense areas while larger complexes, especially those involved in transcription, are primarily localized to the IC or near it. Thus, it could be that chromatin density acts as a regulator of genome function, similar to observations of TAD organization for transcriptionally active (A) and inactive (B) regions of the genome.

Furthering this assertion, it was found that the topography of chromatin domains relaxes during replication by following the live cell through the S phase. Early S phase cells displayed looser, less compact chromatin while mid S phase cells displayed intermediate compaction, followed by the densest chromatin existing in late S phase cells, shown in Figure 5B. PTM histones associated with active transcription were also most enriched in early S phase, while repression associated PTM histones were enriched in later S phase.[95] This example shows that 3D-SIM can be used to determine changes in chromatin compaction and density across replication.

■ RECENT METHODS FOR IMPROVING TARGET LABELING

CRISPR-Based Techniques

Perhaps the most popular method for chromatin tracking in recent times, CRISPR (clustered regularly interspaced short palindromic repeats)-based imaging techniques have been extensively applied in various systems. CRISPR-based imaging techniques utilize RNA and protein expressed from transfected or genomic integrated foreign genes, therefore allowing live-cell chromatin imaging with a minimum perturbation of cellular functions. CRISPR techniques use single guide RNA (sgRNA) that binds to specific DNA targets for assembly of protein−RNA complexes at the target sites. CRISPR-Cas9 was originally used for gene editing, utilizing a nuclease active Cas9 protein to induce double-stranded DNA breaks at a target site. The target sequence could then be excised, and a DNA polymerase would then insert the desired gene sequence.[100] The high specificity of sgRNA binding thus lends CRISPR to usage in sequence-specific imaging.

CRISPR-based imaging systems use a deactivated or "dead" Cas9 (dCas9) protein which lacks DNA cleavage activity but still binds to the sgRNA at the target genes. Binding of the dCas9 is directed by both the sgRNA and the protospacer adjacent motif (PAM) near the DNA target locus. Each PAM is specifically recognized by the corresponding Cas proteins. Upon binding, the Cas protein unwinds the duplex DNA near the target locus and allows for hybridization of the sgRNA.[101] dCas9 is often fused with fluorescent proteins such as GFP or contains modifications that recruit fluorescent proteins, so that binding to sgRNA leads to a rise in the fluorescent signal. The major advantage of a CRISPR-based system is that it allows for the real-time tracking of various genomic targets without introducing foreign DNA with chemical reagents.[102,103] As with FISH, the more probes that bind to a target, the higher the resulting fluorescence. Thus, this system has been used to study regions of the genome with repeating sequences.[104] However, CRISPR techniques are not limited to repeating sequences, as advances in CRISPR system design have allowed researchers to label nonrepeating regions of the genome as well. Below we discuss variations of CRISPR-based imaging that can be used to label repetitive or nonrepetitive sequences.

CRISPR-Based Repetitive or Proximal Sequence Targeting. One of the earliest applications of the fixation-free CRISPR-based techniques was studying telomeric dynamics in live cells. It has been noted by earlier reports[105−108] that longer telomeres have slower movement, but these measurements have relied on either fixative methods, as in FISH, or by tracking fluorescently labeled telomeric binding proteins, such as TRF1 or TRF2, which may affect the natural movement of the telomere. It has been shown that telomere movement occurs through either slow diffusion or directed motion, as seen in Figure 3A. Slow diffusion of telomeres can take several days to diffuse through >1 μm of chromosome territory.[105] The mode of motion exhibited by telomeres may relate to the state of the DNA, as telomere damage has been shown to enhance movement.[109,110] This finding has been supported by the milestone report by Chen et al. using time-lapse microscopy and CRISPR-based confocal live-cell imaging to show that knockdown of TIN2, a telomeric protection protein, leads to an increase in telomere movement; see Figure 3B.[111] The same report also used CRISPR to label subtelomeric repetitive DNA to track replication of sister chromatids.[111] Using dCas9-GFP as the reporter system (Figure 1-4A), HeLa cells were monitored as they prepared for mitosis. Under a confocal microscope, bright signal clusters of telomeres were observed to split into two closely located spots at different times. Duplicate spots were noted to form for each initial signal cluster within 30−60 min between telomere clusters, suggesting that not every chromosome prepares for mitosis at the same time. Another report using a modified version of the dCas9 system that utilized fluorescent proteins to recognize different sgRNA (see Figure 1-4B) successfully tracked the relative positions of telomeres and centromeres

https://doi.org/10.1021/cbmi.4c00033
Chem. Biomed. Imaging 2024, 2, 659−682

during mitosis.[112] Using multicolor labeling of multiple chromosomal loci, it was observed that telomeres and centromeres line up at the metaphase plate and condense as anaphase progressed. Decondensation was observed only after entering telophase and cytokinesis. These reports showed continued signal throughout chromatin condensation and decondensation, which demonstrates the robustness of CRISPR-based techniques and their negligible effects on chromatin dynamics.

Multicolor CRISPR-based chromatin imaging was also achieved by the use of orthogonal CRISPR systems. This method takes advantage of the PAM sequence specificity of Cas9 from different bacteria. Each target tandem repeat sequence in the genome is bound by a sgRNA that contains the PAM sequence of a type of bacteria, while a dCas9 from the same bacteria is coexpressed in the cell and fused to a specific fluorescent protein. The initial report on this method used dCas9 from three bacterial species, *Streptococcus pyogenes*, *Neisseria meningitidis* (Nm), and *Streptococcus thermophilus* (St1), fused to green fluorescent protein (GFP), red fluorescent protein (RFP), or blue fluorescent protein (BFP), respectively. When CRISPR carrying the corresponding PAM of different dCas9's was designed to bind to the telomeric tandem repeat sequence, there was a complete colocalization of different fluorescent protein signals with equal intensity, suggesting the equal binding efficiency and fluorescent efficiency of each orthogonal CRISPR/dCas9 pair.[113] When different CRISPR/dCas9 pairs were used to target subtelomeric and pericentromeric sequences on human chromosomes 9 and 13, coexpression of each pair revealed interchromosomal proximity between the pericentromeric location on chromosome 9 and the subtelomeric location on chromosome 13 as seen in Figure 3C. In the same report, this system was also used to interrogate the proximity of the two intrachromosomal locations on chromosome 9. The signals for the pericentromeric and subtelomeric regions were approximately 2 μm apart, corresponding to the known distance of 75 Mb between the two, signifying the first time two endogenous intrachromosomal loci were interrogated in a live cell.[113] Greater interlocus resolution within 2 Mb was achieved by simply changing the sgRNA for a different locus; thus a dual-color CRISPR system can be used to interrogate changes in chromatin compaction over a short distance.

A common issue with using CRISPR-based techniques that use of multiple fluorescent proteins is the buildup of background signal from protein aggregates. Expression of fluorescent protein must be tightly controlled using clonal cell lines[111,112,114] which can limit the applicability of the technique. This problem can be mitigated through engineering self-associating fluorescent proteins. This approach uses a variant of GFP, superfolder GFP (sfGFP), which is capable of robustly folding into an active protein form in 10 min. sfGFP can be truncated into self-assembling fragments, known as split-sfGFP.[115] However, the self-assembling requirement leads to a low labeling efficiency for small repeating or nonrepeating loci; thus this technique cannot be utilized in cell lines with low transfection efficiency. The technique also needs a high level of sgRNA expression to compensate for the low level of fluorescent protein; thus usage with endogenous expression vectors is best. To amplify the signal level from low levels of protein fluorescence, the SunTag system can be utilized to localize reconstituted split-GFP protein to the genomic target. SunTag, or SUperNova Tag, utilizes a polypeptide containing multiple repeats of an epitope that are recognized by single-chain variant fragments (scFv's) of antibodies that are themselves fused to fluorescent proteins, such as GFP.[116] By fusing the SunTag to dCas9, a split-sfGFP fragment fused with scFv's can bind to the SunTag and recruit the other fragments of split-sfGFP to reconstitute the full fluorescent protein (see Figure 1-4C). Fusing a split-sfGFP fragment that does not have the scFv to another fluorescent protein, such as mCherry, would thus lead to a dCas9 complex that, when complete, has multiple fluorescent proteins. mCherry can be tagged with the portion of MCP (MS2 coat protein; see below) that binds a specific RNA stem-loop motif integrated into the sgRNA. Because the sgRNA binds specifically to the genomic target, mCherry fluorescence can be used to verify localization of the dCas9 complex and subsequent split-GFP fluorescence to the genomic target. The combination of both mCherry and split-sfGFP fluorescent proteins leads to 9- and 13-fold reductions in background fluorescence levels as compared to the standard dCas9-EGFP and SunTag sfGFP systems.[117] This is due to the individual fragments of split-GFP not being fluorescent until assembled. The SunTag split-sfGFP system leads to clear foci in 40−60% of cells and provides a higher signal-to-background ratio and lower fluorescence intensity than either the dCas9-EGFP or SunTag sfGFP complexes; see Figure 3D.

The combination of SunTag and split-sfGFP has been used to specifically track the diffusion dynamics of chromosome 9 by targeting the pericentromeric region. The SunTag split-sfGFP system exhibited 10-fold lower fluorescence signal but with almost no background fluorescence, which was attributed to reversible association of the split GFP fragments. In addition, this system also exhibited the slowest signal decay over time, as well as fluorescence recovery after photobleaching of 10−20 min. The slow rate of signal decay allows for the determination of chromatin movement over time. Analysis of the movement calculated from 2D trajectories of chromosome 9's pericentromeric region revealed different modes of movement, with subdiffusive motion over short time scales and actively driven motion over longer time scales. These trajectories can be seen in Figure 3D. Subdiffusive motion may be due to nuclear confinement or conformational constraints as a result of higher chromosomal structure. This difference in movement is consistent with earlier reports on the differences in dynamic motion for telomeres, validating the efficacy of newer techniques in the tracking of chromatin movement. Although the SunTag split-sfGFP system can provide details of chromatin motion, it is an intensive technique, requiring the expression of four proteins for single-color genome imaging which consequently lowers the applicability of this technique toward multicolor imaging.

Other modifications of the CRISPR-dCas9 system can potentially solve the issue of incorporating multicolor imaging. One system, reported by Fu et al.,[114] involves three components: dCas9, sgRNAs that contain stem loops attracting protein binding, and RNA binding proteins fused to fluorescent proteins (see Figure 1-4C). The stem loops used in their study are derived from motifs bound by the bacteriophage coat proteins MCP (MS2 coat protein) and PCP (PP7 coat protein).[114] Thus, sgRNA containing either of the corresponding stem loops will recruit either MCP or PCP that is tagged with EGFP or mCherry, respectively. The components of this system can be introduced simultaneously or individually, with special consideration for individual introduction. For individual introduction of each component,

https://doi.org/10.1021/cbmi.4c00033
Chem. Biomed. Imaging 2024, 2, 659−682

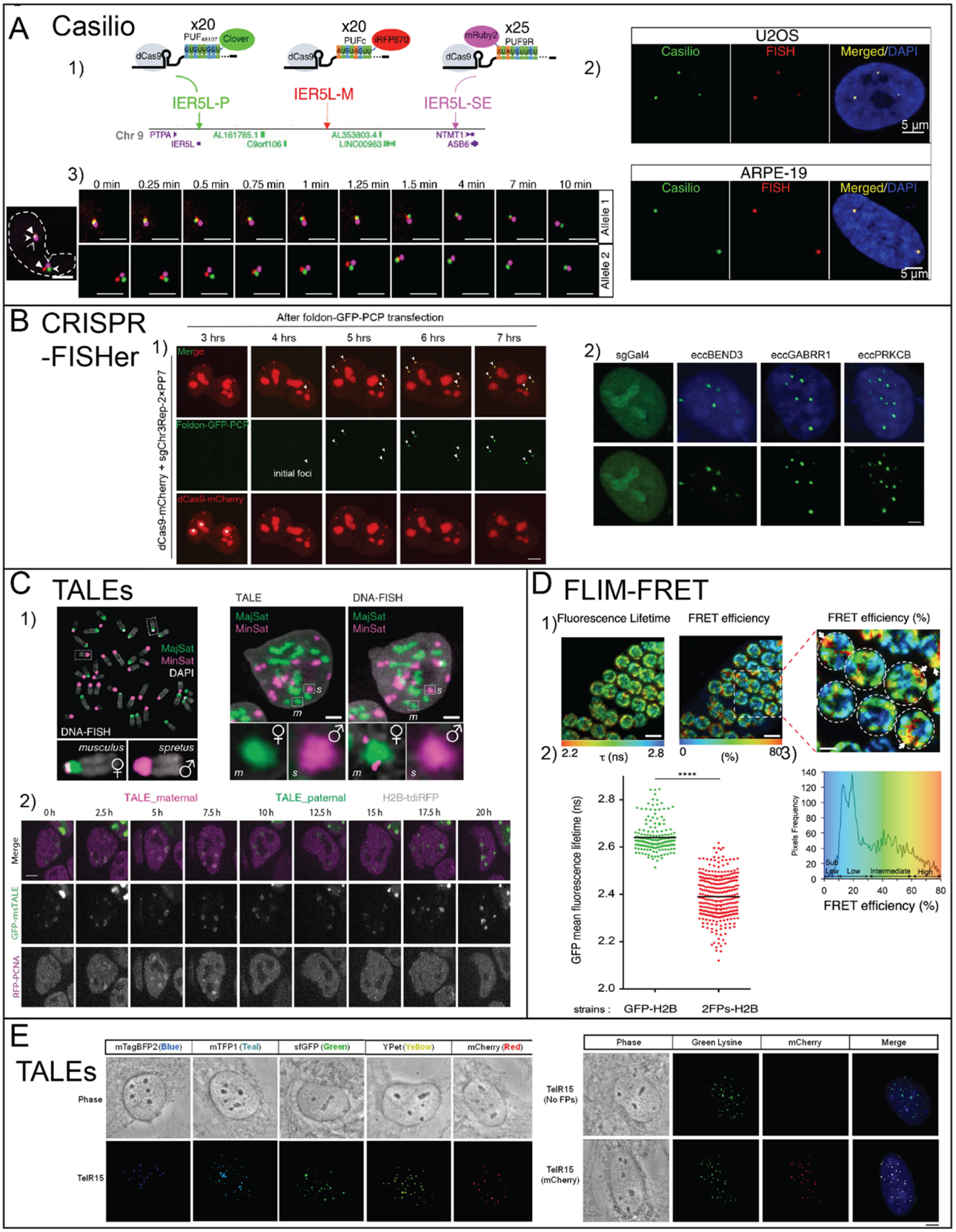

Figure 4. CRISPR techniques continued, TALES, and FLIM−FRET. (A) (1) Schematic showing Casilio construct design for studying the loop between the *IER5L* promoter (IER5L-P) and its superenhancer (IER5L-SE), midpoint marked by IER5L-M. *N* number of PUF-domains are used to localize to different genomic loci for multicolor imaging. (2) Colabeling of MUC4 locus by Casilio (green) and DNA-FISH (Cy5-MUC4, red) in U2OS cells shows a 96% overlap between methods, while colabeling in ARPE-19 cells shows a 100% overlap. Scale bar, 5 μm. (3) Representative nucleus (nuclear boundaries outlined) and time-lapse images of *IER5L*-P-SE loop, with *IER5L* promoter, midpoint, and superenhancer labeled by Clover (green), iRFP670 (red), and mRuby2 (magenta) between two alleles of *IER5L*. Reproduced in part with permission from ref 123. Copyright

https://doi.org/10.1021/cbmi.4c00033
Chem. Biomed. Imaging 2024, 2, 659−682

Figure 4. continued

2022 Clow et al. (B) (1) The enrichment of foldon-GFP-PCP at the Chr3Rep loci (white arrows) labeled by dCas9-mCherry in live U2OS cells. Foldon-GFP-PCP foci started to occur ∼4 h post transfection. The stars show nucleolar dCas9-mCherry accumulation. (2) Representative images of labeled eccDNAs by CRISPR FISHer in HepG2 cells with sgGal4 as a control. Reproduced in part with permission from ref 126. Copyright 2022 Lyu et al. (C) (1) TALES imaging of murine major and minor satellites. (left) DNA-FISH for MajSat (green) and MinSat repeat (magenta) with chromosome spreads of SF1 ES cells. (right) Images of SF1 cells expressing TALE-mClover for the major satellite (green) and TALE-mRuby2 against *M. spretus* MinSat sequence (magenta) compared to DNA-FISH for the major and minor satellites. Close-up views of boxed areas for *M. spretus* (s) and *M. musculus* (m) are shown at the bottom. Scale bars, 1 μm. Reproduced in part with permission from ref 137. Copyright 2013 Miyanari et al. (2) Cell-cycle-dependent distribution of GFP-msTALE with live-cell imaging of a replicating stable GFP-msTALE cell line (green) stably transfected with RFP-PCNA (magenta) as a control. Reproduced in part with permission from ref 138. Copyright 2014 Thanisch et al. (D) (1) FLIM (left) and FRET (right) images of 2FPs-H2B cells. Scale bars, 5 μm. Magnification shows regions with distinct FRET efficiencies. White arrows highlight specific high-FRET regions. Meiotic nuclei are outlined with dashed lines. Scale bar, 2 μm. (2) (left) Scatterplots show the mean GFP fluorescence lifetime distribution in GFP-H2B (green diamonds; 195 cells, n = 7 gonads) and 2FPs-H2B (red diamonds; 327 cells, n = 10 gonads) worms. ****, $p < 0.0001$ (two-tailed Mann−Whitney test); 95% confidence interval. (right) FRET efficiency variation graph showing distinct populations. Low (in blue), FRET efficiency between 10 and 30%; intermediate (in green), FRET efficiency between 30 and 60%; and high (in orange), FRET efficiency between 60 and 80%. Reproduced in part with permission from ref 88. Copyright 2017 Lleres et al. (E) (left) TALE-TelR15 probes were designed with various fused fluorescent proteins and transfected into fixed U2OS cells. (right) TALE-TelR15 probe with no fused fluorescent protein but with internally labeled lysine residues (upper row) was used to compare with the same TALE carrying fused mCherry (lower row) to demonstrate overlap of the localization signal. The far right column merges respective images overlaid onto DAPI images. Scale bar on right, 5 μm. Reproduced in part with permission from ref 141. Copyright 2013 Ma et al.

a stable cell line must first be established, treated for dCas9 selection using puromycin, and then cells expressing both fluorescent proteins must be carefully selected to ensure the optimal level of signal fluorescence. As previously discussed, too high protein fluorescence invariably leads to higher levels of background fluorescence, which is not suitable for visualization of target loci. To assess the viability of this system, the murine major satellite region in the pericentromere served as a target because major satellites form a complex three-dimensional structure known as pericentromeric heterochromatin (PCH).[118] PCH can be easily identified using DAPI staining allowing for comparison with CRISPR-based imaging systems. The pericentromere also serves as a simple target locus to validate this system as it is 6 Mb of a 234 bp repeating sequence, which would increase the number of sgRNAs that can hybridize to it, leading to an increase in fluorescence.[119−121] Hybridization of sgRNA containing the MS2 stem loop recognized by MCP led to localization of the MCP-EGFP complex to this locus, revealing a distinct signal with low background fluorescence that was validated by FISH labeling using probes specific to the pericentromere. Likewise, hybridization of sgRNA containing the PP7 stem loop led to localization of the PCP-mCherry complex whose signal was also validated by FISH. Comparing the two complexes to the standard dCas9-EGFP complex, where EGFP was directly tagged to the dCas9, revealed similar signal-to-background ratios, supporting the efficacy of this labeling system.

With slight modifications of the sgRNA, this system can also be used for dual-color live imaging. The sgRNA for the PCP-mCherry complex can be modified to target the major satellite region of the mouse chromosome while the sgRNA for the MCP-EGFP complex selects for the minor satellite. The minor satellite is approximately one-sixth the size of the major satellite, at around 0.6−0.12 Mb.[122] Dual labeling of each satellite validates the performance of this system but demonstrates the sequence specificity CRISPR-dCas9 systems offer. Indeed, imaging of both fluorescent protein complexes reveals localization of two MCP-EGFP signals at the minor satellites and one larger PCP-mCherry signal in between. Organization of the labeled centromeric regions can also be tracked through the cell cycle using this method, revealing scattered chromosomes in prophase and aligned chromosomes in metaphase. Interestingly, in anaphase, the EGFP signal at the major satellite lowers and recovers during telophase. The mCherry signal, targeting the major satellite, also changes, going from large distinct puncta to a more diffuse smeared signal as highlighted in Figure 3E. These findings highlight the differences in chromatin compaction during the cell division.

The advantages of dual labeling come into play when studying epigenetic regulatory mechanisms where two loci interact or changes in chromatin configuration during cell replication. Additionally, this technique utilizes dCas9 from a single species, *S. pyogenes*, which contains a simple PAM region. The PAM for *S. pyogenes* consists of the NGG motif, which is ubiquitous throughout the genome and thus can be used to label almost any genomic locus. Thus, this variation of CRISPR retains high flexibility and can be expanded upon for tricolor imaging by using various RNA motifs within the sgRNA to recruit proteins fused with other fluorescent proteins.

CRISPR-Based Nonrepetitive or Distant Sequence Targeting. Thus far, most variations of CRISPR have relied on localization of multiple sgRNAs to a single locus in order to achieve enough signal intensity for imaging. This requires sequences with either close proximity or repetition of the target sequence. For imaging of targets with nonrepetitive sequences, multiple sgRNAs would be needed to achieve the same signal intensity as in repetitive sequences. To tackle this, work has been done to achieve imaging-quality signal using only one sgRNA per locus on nonrepetitive sequences. The modular Casilio platform, dCas9-Pumilio/FBF(PUF), combines the versatility of PUF domains with the multimerization of effector molecules.[123] PUF is the shared RNA-binding domain of Pumillio and FBF proteins that can be programmed to bind a specific RNA sequence of 8 nt long. The effector domains, which are the protein domains that achieve a specific function, are fused to a PUF RNA binding domain. The PUF binding domain then binds to one or more repeats of a specific 8 nt motif on the 3′ end of an sgRNA through contacts made between tunable RNA-base specific amino acids within the PUF domain and the RNA. In this way, over 65 000 (4^8) effectors are possible for a wide range of potential genomic loci. A schematic of this system is shown in Figure 4A1. The Casilio system was validated in its nonrepetitive locus labeling

https://doi.org/10.1021/cbmi.4c00033
Chem. Biomed. Imaging 2024, 2, 659−682

capacity by comparing it with FISH to label the *MUC4* gene on chromosome 3, shown in Figure 4A2. This gene has a region of nonrepetitive sequence and a region of repetitive sequence, which makes it ideal to compare between the two techniques. Comparing the overlap between Casilio and FISH labeling reveals near-perfect colocalization between the two signals, with comparable intensity between the two as well. However, while FISH requires hybridization with many individual fluorescent probes, imaging with Casilio requires the binding of one sgRNA with 15 copies of a PUF binding site (PBS) to recruit 15 PUF domains, each tagged with a fluorescent protein. Importantly, dCas9 is required for formation of the Casilio complex, as omitting it would not allow for hybridization of the sgRNA to the target DNA locus. Simply put, Casilio achieves with one sgRNA what FISH requires 15 individual probes to do.

The Casilio system has also been used to track chromatin interactions using a two-color system. The *MASP1*−*BCL6* loop has 362 kb of genomic distance between the two loci. Using sgRNAs to bind to nonrepetitive locations near the loci, dynamic interactions between these genomically far loci were uncovered. Within a single cell, interactions between *MASP1* and *BCL6* were inconsistent across allelic pairs. At the beginning of imaging under a confocal microscope, it can be seen that the two labeled loci are approximately 1 μm apart, but as imaging continues, one allelic pair remains fairly consistent in the distance between loci, whereas the other drifts to approximately 1.5 μm apart.[123] Besides studying the interactions between far genomic loci, Casilio can be applied to study protein effects on chromatin compaction as well. Depletion of RAD21, a vital protein in cohesin complexes, in cells has been shown to result in the loss of loop domains in chromatin. This includes a large (approximately 500 kb) loop between the nonrepetitive IER5L promoter (IER5L-P) and its superenhancer (IER5L-SE). Labeling these two loci allows for the monitoring of the distance change as a function of RAD21 depletion. Indeed, depletion of RAD21 in HCT116 cells leads to farther distances between pairs of labeled promotors and enhancers, with distances between loci increasing to 2.09 μm from 1.21 μm. This finding using Casilio validates the earlier reported effects of RAD21 depletion that had been found using Hi-C.[124,125]

Chromatin dynamics can also be tracked with Casilio in a three-color configuration as seen in Figure 4A3. Imaging in this way mimics STORM, where multiple sequentially binding probes are used to reconstruct the imaged target. Here though, each sgRNA recruits a differentially tagged fluorescent protein to track the "live" structure of a target. This variation of Casilio is known as PISCES (Programmable Imaging of Structure with Casilio Emitted sequence of Signal).[123] PISCES allows for real-time monitoring of nonrepetitive sequence structural dynamics. These dynamics can then be tracked either in real time or with the use of time-resolved microscopy.

Overall, Casilio represents a variation on the classical CRISPR-dCas9 system that has increased specificity, a significantly reduced sgRNA need, and simpler transfection protocols, and it can track changes in chromatin location within 1 μm, with applicability in studying the effects of protein depletion and replenishment. However, the potential disruption of natural dynamics is an ever-present concern when using CRISPR-based techniques, as the expression of sgRNA and various proteins can potentially disrupt native interactions in the targeted loci. The Casilio system is not immune from these concerns, but there is potential for these challenges to be at least partially overcome with more careful sgRNA design and smaller, more optimized fluorescent proteins.

Further expanding on labeling of nonrepetitive sequences, a combination of both CRISPR and FISH has arrived to achieve the best of both techniques. CRISPR FISHer, or CRISPR-mediated fluorescence *in situ* hybridization amplifier, takes traditional CRISPR-dCas9 techniques and combines them with phase separation based assembly of fluorescent proteins.[126] This can confer enhancements in both signal intensity and signal-to-background ratio through the formation of phase separated regions containing the fluorescent protein, concentrating the fluorescence signal at the target locus. CRISPR FISHer has been used to visualize, in real time, the entire process of chromosomal damage, separation, and subsequent end joining in a single live cell. This system utilizes dCas9, but notably the sgRNA contains two PP7 RNA aptamers that recruit a fusion trimeric protein consisting of PCP, GFP, and a T4 fibritin trimeric motif foldon (complex termed foldon-GFP-PCP). The use of fibritin foldon stems from its ability to keep protein complexes stabilized and soluble.[127,128]

The foldon-GFP-PCP and sgRNAs containing two to eight repeats of PP7 were shown to form small condensates, which may suggest that assembly of this CRISPR-based complex induces phase separation due to multiple contacts between protein and sgRNA (see Figure 4B1). This would then lead to increased GFP fluorescence intensity at these loci. For example, in the report by Lyu et al., transfection of this system in osteosarcoma U2OS cells showed foci at *Chr3q29*, colocalized with marker dCas9-mCherry.[126] The intensity of the foldon-GFP-PCP complex increased with time without a corresponding increase in the mCherry signal. This may indicate recruitment by the dCas9-mCherry of the foldon-GFP-PCP complex to the target locus. This system can also tackle repetitive sequences, such as the telomere, and does so with increased sensitivity over other CRISPR-based imaging systems, due to condensation of the fluorescent protein during phase separation. However, this does raise the concern as to perturbation of natural chromatin dynamics. For tracking of endogenous nonrepetitive regions of DNA, sgRNA designed to target *PPP1R2* loci and both the foldon-GFP-PCP and dCas9-mCherry systems were transfected into U2OS cells. Only the foldon-GFP-PCP complex was observed to localize to the target loci, proving the suitability of CRISPR FISHer to target nonrepetitive regions in live cells.[126]

For monitoring of DSB and subsequent repair by non-homologous end joining (NHEJ), *PPP1R2* was labeled using CRISPR FISHer at two different loci, one with GFP and the other with MCP-tdTomato, a red fluorescent protein. These two red and green loci would thus be in close proximity before the induction of DSB and separate afterward. Introduction of cleavage active Cas9 caused the red and green signals to separate as expected, and then rejoin, likely a result of CRISPR-mediated cleavage followed by NHEJ-mediated repair. CRISPR originally arose as a method of gene editing, selectively targeting DNA to be excised and the resulting gap in DNA filled in with the desired sequence. Using CRISPR FISHer, that process has now been monitored in real time in live cells.

CRISPR FISHer also has the capacity to detect a historically difficult DNA element: extrachromosomal circular DNA

https://doi.org/10.1021/cbmi.4c00033
Chem. Biomed. Imaging 2024, 2, 659−682

elements (eccDNAs). eccDNAs have been known since 1964 and can range in size from hundreds to millions of bases. Certain eccDNAs, such as extrachromosomal DNA (ecDNA), range in size from 50 kb to 5 Mb and are thus detectable by DNA-FISH. However, other eccDNAs are much smaller and thus harder to detect using traditional methods. eccDNAs are thought to play a role in gene regulation, immune responses, and intracellular communication.[129−131] To study the localization of eccDNAs, known eccDNAs were sequenced to design sgRNAs to target the junction sequences (where the two ends of formerly linear DNA meet to circularize) of the eccDNAs because these sequences are not elsewhere present in the genome. Tracking of individual eccDNA loci revealed a further traveling distance and 3D space than simultaneous tracking of chromosome 3, indicating that eccDNAs are more highly dynamic, with longer trajectories and faster speeds (see Figure 4B2).

Transcription Activator-like Effector (Nuclease) (TALE(N))

Transcription activator-like effector nuclease (TALEN) techniques operate similarly to CRISPR techniques in that they both are programmable nucleoprotein complexes that were initially created for target-specific editing.[132] While CRISPR systems localize to their target locus though their unique PAM motifs and sgRNAs, TALEN systems utilize a DNA-binding domain (DBD) containing tandem arrays of approximately 30 amino acid long monomers. These monomers can be customized to recognize theoretically any genetic sequence.[133,134] Upon binding of the TALEN to the target locus, the nuclease region can then cleave the DNA sequence, leaving a dsDNA break than can be repaired by endogenous repair systems.[135,136] Like CRISPR imaging techniques that use a deactivated or "dead" Cas9 to localize to a genomic target, modifying TALEN for imaging involves removing the nuclease domain, referred to as TALEs. TALEs has been used in live cells for imaging complex chromatin dynamics much like CRISPR.

For example, due to the high specificity and programmability of the DBD, TALEs has been used to study single-nucleotide polymorphisms (SNPs) in mouse centromeres *in vivo*.[137] As mentioned earlier, pericentromeres contain a tandem repeat region known as the major satellite that can be readily stained by DAPI. TALEs were designed to recognize various repeats of the major satellite sequence and were labeled with the GFP mClover. The targeting ability of the TALEs constructs was validated by colocalization of FISH-labeled major satellite with the mClover TALEs signal. Using hybrid stem cells between *Mus musculus* and *Mus spretus*, TALEs was able to distinguish four SNPs between each parent. The relative abundance of targeted major and minor satellite sequences was also found to differ between parental chromosomes. *M. spretus* had higher amounts of minor satellite repeats, while *M. musculus* had more major satellite repeats. FISH confirmed most of these findings, but interestingly was almost unable to detect major satellite regions in *M. spretus*. Using two color TALEs, one tagged with mClover and the other tagged with mRuby2, researchers were able to distinguish maternal and paternal chromosomes in the hybrid ES cells, as shown in Figure 4C1. In this experiment, TALE-mClover was designed against the major satellite in paternal *M. spretus* while TALE-mRuby2 was specifically designed to localize to two SNPs in the minor satellite only present on the maternal *M. musculus*. It was found that TALE-mRuby2 did not localize to the paternal minor satellite at all, binding solely to the minor satellite of the maternal chromosome, demonstrating the remarkable specificity of TALEs to distinguish between similar genomic targets.

TALEs has also been used to track murine pericentromeric chromatin during the cell cycle *in vivo*.[138] In this study, GFP fused TALEs (TALEs-GFP) designed against the major satellite region were endogenously expressed along with H2B-RFP to track localization of the DNA within nucleosomes across the nucleus. Cells were observed over 20 h at 150 min intervals and revealed that TALEs-GFP was located at replication foci in mid to late S phase, as shown in Figure 4C2. Through mitosis, TALEs-GFP remained localized to chromosomes until midprophase, dissociated, and then reassociated in early telophase. The dissociation may be due to chromatin condensation forcing dissociation of the TALEs from the DNA. Better design of TALEs binding may prevent such an issue in future studies. TALEs was further followed to determine the kinetics of binding to the chromatin and was found to have a higher fluorescence recovery after bleaching (FRAP; see Lippincott-Schwartz et al.[139] and Phair and Misteli[140]), indicating highly transient binding dynamics.

TALEs can also effectively target telomeres.[141] TALEs fused to various fluorescent proteins can be designed to localize to either of the telomeric strands. These TALEs exhibited discrete foci in interphase cells, and as expected, doubled in number between G1 and G. However, the number of foci was less than expected, as less than 50 labeled foci were observed per nucleus which is consistent with the transient binding dynamics discussed earlier. Ma et al.[141] were able to endogenously express five differently fluorescently labeled TALEs to study various aspects of chromatin movement in live cells, shown in Figure 4E. They were also able to transfect fluorescent TALEs in a manner similar to FISH probes, demonstrating the flexibility of the TALEs method for both imaging in both live and fixed cells. Using TALEs, they were able to detect and bin telomeres of differing lengths in different chromosomes.

Overall, TALE-based techniques are flexible and decently simple to implement. Their applicability in live and fixed cells lends itself to a variety of biological questions. The main drawback of this method is that they exhibit transient binding and signal loss may accumulate when chromatin undergoes significant organizational changes.

MODERN METHODS FOR NUCLEUS-WIDE CHROMATIN DYNAMICS

Single Nucleosome Imaging

Thus far, the techniques discussed have addressed imaging techniques that track multiple nucleosomes or larger clusters of chromatin across the nucleus. However, work has been done by multiple groups on tracking single nucleosomes. Nozaki et al.[78] combined PALM with single nucleosome tracking to observe compact domains in mitosis in live cells with dynamics affected by chromatin associated factors as well as internucleosomal interactions. By replacing histone protein H2B with a modified version of H2B fused to PA-mCherry (H2B-PA-mCherry), researchers were able to use PALM to observe a thin section of a single nucleus that had distinct spots with a single photobleaching event per spot. The single-step photobleaching event suggests singular incorporation of the modified H2B into a nucleosome. Recording these nucleosomes using live-cell PALM revealed tight clusters of

https://doi.org/10.1021/cbmi.4c00033
Chem. Biomed. Imaging 2024, 2, 659−682

nucleosomes, with more clustering along the nuclear periphery, consistent with observations using Deep-PALM (see Deep Learning Based Super-Resolution Imaging). The observed sizes of these clusters ranged from 160 nm in diameter in fixed cells to 220 nm in live cells, which is consistent with the known phenomenon of fixation influencing native chromatin structure and condensation.[142] This finding both demonstrates the imaging accuracy of live-cell PALM and highlights an important consideration when studying chromatin structure in fixed cells. Nozaki et al.[78] have also used their single nucleosome imaging technique to study chromatin dynamics in live cells and found that, over an observation time of 500 ms, there were a variety of different chromatin movements. First, consistent with earlier reports,[143] it was noted that, within 50 ms, nucleosome movement of 60 nm was observed. Second, comparing movement of H2B-PA-mCherry with a known marker for DNA replication, Cy3 labeled dCTP, showed that the DNA replication domains and the nucleosomes in close proximity have a correlation in movement. This observation indicates that movement of individual nucleosomes reflects the movement of a nearby DNA replication domain. Third, analysis of heterochromatin movement along the nuclear periphery revealed shorter movements as opposed to longer movements observed deeper within the nucleus. This lack of long-range movement of chromatin at the periphery indicates adhesion of chromatin to inner membrane structures, as reported earlier.[144,145]

Perturbing the natural environment of the live cells by changing internucleosome interactions revealed differential modes of chromatin movements. Treatment of live cells with Trichostatin A leads to an overall increase in chromatin movement distance as opposed to nontreated cells. As Trichostatin A inhibits binding of the H3 and H4 tails to neighboring nucleosomes, the increase in movement most likely reflects a significant decrease in chromatin compaction.[20] The shorter distances traveled by nucleosomes at the nuclear periphery were almost abolished, and the total area covered throughout the nucleus increased. siRNA treatment to deplete RAD21, a component of the cohesin complex, revealed similar results.[78] Cotreatment resulted in overall higher effects on chromatin mobility than either treatment. These results thus suggest that interactions between nucleosomes influence chromatin domain formation and restrict their dynamics.[78]

Single nucleosome live-cell PALM imagining of embryonic stem cells during cell differentiation revealed less condensed chromatin, thus poorly defined structure, and higher dynamics when compared to HeLa cells. After differentiation, while the volume of chromatin did not change, the chromatin domains themselves became more defined with fewer dynamics as opposed to during differentiation. These findings would suggest that the process of differentiation of stem cells requires more decondensation of chromatin than in cancer cell division. Thus, chromatin in pluripotent cells is inherently more dynamic than chromatin in somatic cells.[20,146]

Further work on single nucleosome movement by Lerner et al. used a two-parameter analysis to resolve low to high mobility of chromatin domains with different localization patterns.[147] By tracking individual H2B proteins, the researchers were able to define two parameters to characterize chromatin movement: (1) the average displacement of each tracked nucleosome measured in nanometers over the detection time, which would give the average speed of the nucleosome, and (2) the radius of confinement, effectively the circle of movement of the tracked nucleosome before it encounters another tracked nucleosome within the same space.[148] These two parameters positively correlate with each other for the most part; however, deviations between the two parameters indicate that the nucleosome may move quickly within a small area or move slowly in a large area. The interplay between these two parameters allows for the classification of differing mobility chromatin into five distinct states, from very low to very high mobility. These five mobility states have been observed across different cell types with similar distributions. The most notable difference comes from the low mobility chromatin, which was nearly absent in pluripotent cells, consistent with the higher chromatin dynamics reported in the work above. This method was also used to further support the assertion of interaction of nucleosomes at the nuclear periphery with nuclear lamina proteins such as lamin-A at lamin-associated domains (LADs).[149]

The two-parameter tracking method can also be applied to other proteins associated with chromatin to assess their mobilities. The heterochromatin epigenetic reader proteins HP1α, HP1β, and HP1γ along with the heterochromatin writers SUv39h1 and SUv39h2 each expressed different patterns of mobility across the nuclear space. Analysis of each protein's mobility distribution revealed that regulators of heterochromatin had higher levels of interaction with lower mobility chromatin, which would suggest that the lower mobility is due to active repression of its dynamics by these regulators. Interestingly, a difference in mobility patterns exists among the isoforms of HP1. β and γ were abundant in low mobility chromatin but not in very low or intermediate chromatin, whereas α was abundant in the high mobility chromatin. It could be possible that the isoform behavior represents differences in heterochromatin regulation.

Using the two parameters of displacement and confinement radius can define a mobility landscape that is modulated by the associated transcription, binding, and organization factors that differentially associate with heterochromatin. This technique is undoubtedly powerful in its ability to highlight associations between chromatin accessibility and localization, surpassing what diffusion-limited techniques can determine.

Dense Flow reConstruction and Correlation (DFCC)

While most methods of tracking chromatin movement are qualitative, work has been done on quantifying the overall chromatin movement in the whole nucleus. Most methods of quantification focus on optical flow (OF), which estimates 2D movement of pixels between two consecutive images and assigns a displacement vector to those pixels.[150] The error in OF methods is typically evaluated using the angular error (AE) and end point error (EE), which reflect errors in direction and magnitude of movement, respectively. Overall, most OF methods such as Horn−Schunck formulations,[151] particle image velocimetry (PIV),[152] phase-based methods,[153] or SIFT-based methods[75] develop higher AE and EE at labeling densities close to 1/px and increasing number of independently moving domains and overall decreasing AE with faster diffusion coefficients.

One such method that achieves smaller AE and EE than other methods is Dense Flow reConstruction and Correlation (DFCC), which provides vectorial information below the diffraction limit with a resolution of approximately 65 nm.[154] This method has been used to analyze movements of

https://doi.org/10.1021/cbmi.4c00033
Chem. Biomed. Imaging 2024, 2, 659−682

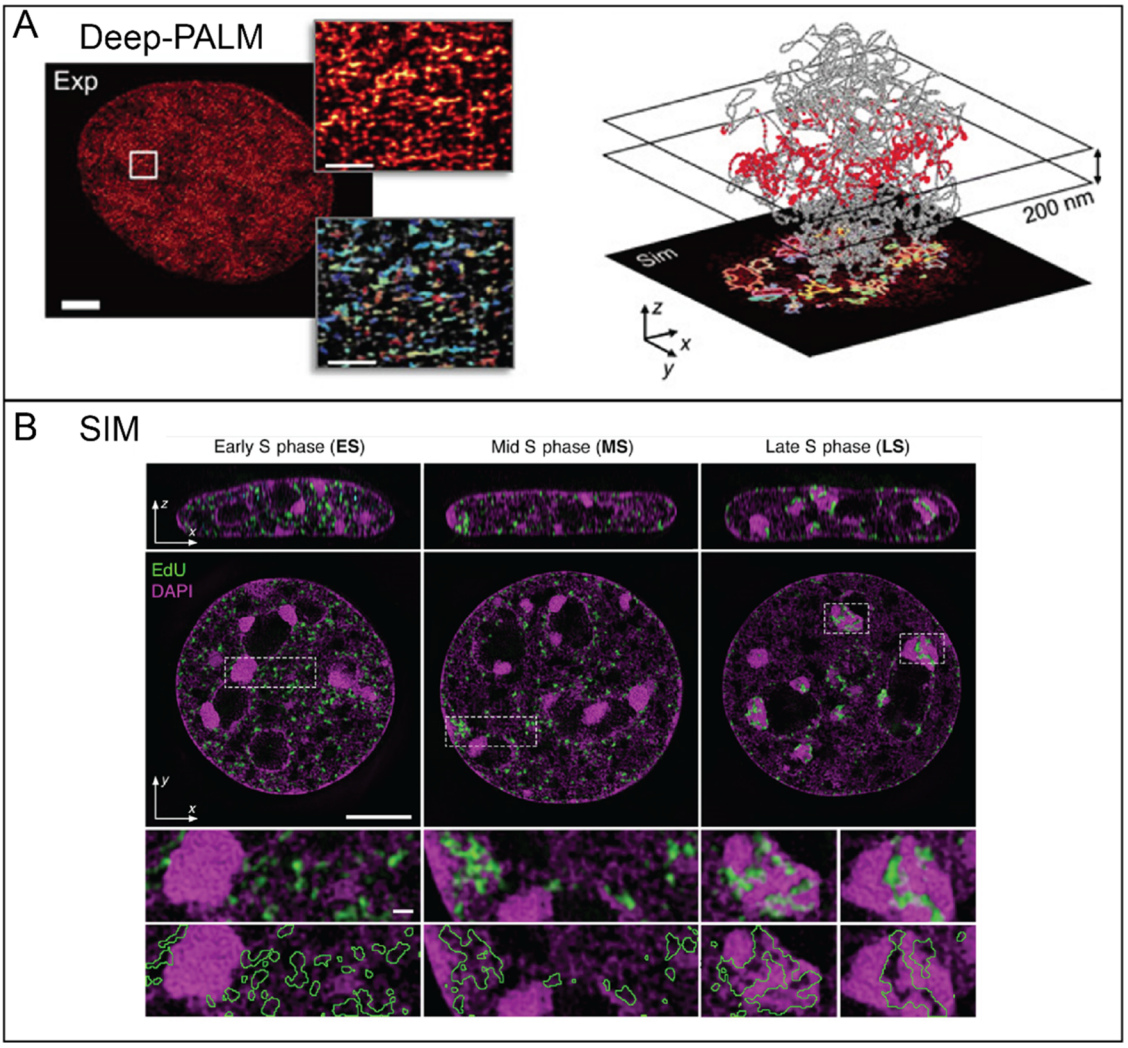

Figure 5. Deep-PALM and SIM. (A) (left) Super-resolved images show blobs of chromatin. These blobs are segmented and individually labeled by random color (magnifications on right). Scale bars, 2 μm (whole nucleus); magnifications, 200 nm. (right) Generation of super-resolution images and blob identification and characterization for a segment of chromosome 1 from GM12878 cells. Beads of a 5 kb genomic length of a simulated polymer are projected to the imaging plane within a 200 nm thick slab, resembling experimental super-resolved images of live chromatin. Reproduced in part with permission from ref 77. Copyright 2020 Barth et al. (B) Orthogonal (top) and lateral (middle and bottom) cross sections of representative 3D-SIM data sets showing the different patterns of replication foci (green) during progression from early (ES), mid (MS), and late S phase (LS) stages (left to right). Chromatin is stained with DAPI, and replication is labeled using 15 min of EdU incorporation. Local replication regions were masked based on the EdU signal and outlined in green. Scale bars, 5 and 0.5 μm (middle and bottom rows, respectively). Reproduced in part with permission from ref 95. Copyright 2020 Miron et al.

chromatin across the whole nucleus in transcriptionally active and inactive cells. In the work by Shaban et al.,[154] DNA was stained using the cell-permeable DNA probe SiR-Hoescht (also known as SiR-DNA) while histones were labeled using H2B-GFP as described earlier. In transcriptionally active nuclei, the movement of both the DNA and the histones were correlated over a large distance of 11 μm by 18.2 s. The movements of chromatin across nuclei can be used to create flow fields, which illustrate the local movements of tracked chromatin over the observation time. Examples of these flow fields can be found in Figure 6A. Flow fields for transcriptionally active nuclei reveal vortex-like movements of chromatin spanning a few hundred nanometers, evenly dispersed across the nucleus. These vortexes may represent local remodeling of the chromatin by various transcription related effectors.[155,156] This submicron movement is not easily visualized using other methods but is made possible by DFCC.

Displacement Correlation Spectroscopy (DCS)

Displacement correlation spectroscopy (DCS) allows for the mapping of interphase chromatin dynamics in live cells at the micron level by combining PIV (see earlier) and cross-correlation between image pairs to vectorially measure local chromatin movements.[157] At a lateral resolution of 65 nm at 250 ms/frame, H2B-GFP was imaged in 25 s sequences to reveal coherent movement over micron-scale regions of the nucleus lasting under 10 s. Interestingly, this method has shown that the direction of movements is not uniform across the nucleus and loses coherency over longer time scales. These findings suggest that the movement related to transcription or preparation for mitosis is not uniform, with different chromosomes being manipulated at different times. When ATP was depleted from the cell, the bulk of chromatin movements were abolished entirely, suggesting that the chromatin movement is ATP dependent. While this may

https://doi.org/10.1021/cbmi.4c00033
Chem. Biomed. Imaging 2024, 2, 659−682

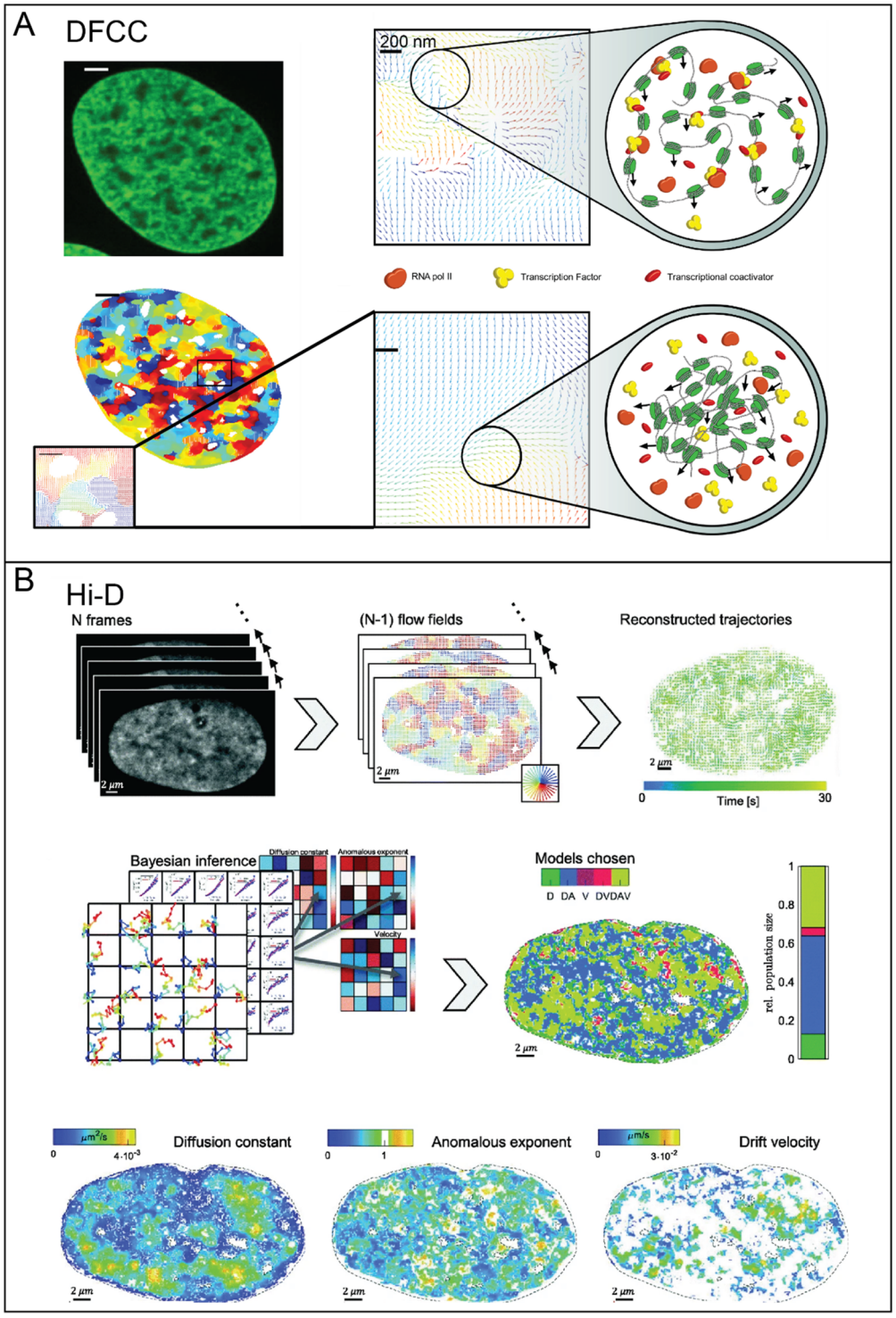

Figure 6. (A) (top left) Fluorescence microscopy image of a nucleus expressing H2B-GFP. Scale bar, 3 μm. (bottom left) Flow field for time between images = 0.2 s and zoomed-in region (inset); the field is color-coded according to the direction of the displacement. Scale bar, 3 μm (bottom left) and 1 μm (inset). (right) Representative magnification of flow fields illustrating changes in direction and smoothness (coherency of motion, black arrows) between serum stimulation (top) and starvation (bottom). Low smoothness in the bottom map may reflect chromatin decompaction in starved cells. Reproduced in part with permission from ref 154. Copyright 2018 Shaban et al. (B) (top) A series of 150 confocal microscopy images acquired at 5 fps (left) are subjected to dense optical flow to define flow fields of the images (center) based on the fluorescence intensity of each pixel. Individual trajectories are reconstructed over acquisition time (right). (middle) Trajectories of a 3 × 3 pixel neighborhood are used to calculate a mean MSD curve and its covariance matrix. Using Bayesian inference, the diffusion type best fitting each curve is chosen (free diffusion (D), anomalous diffusion (DA), directed motion (V), or a combination (DV or DAV). The distribution of each pixel's model is shown as a color map (right). (bottom) Maps of biophysical parameters (D, a, and V) extracted from the best describing model per pixel. Reproduced in part with permission from ref 158. Copyright 2020 Shaban et al.

https://doi.org/10.1021/cbmi.4c00033
Chem. Biomed. Imaging 2024, 2, 659−682

suggest that movement is being driven by ATPases, what was observed was an apparent compaction of chromatin, which would suggest that ATP is required to maintain the less compact and transcriptionally active chromatin that is mobile. Further supporting this finding was the addition of multiple drugs known to inhibit replication and transcription machinery strongly inhibiting coherence but increasing local displacements. This would mean that addition of these drugs does not stop chromatin movement, but now the chromatin moves diffusely, leading to decondensation of chromatin.

High-Resolution Diffusion Mapping (Hi-D)

Building from DFCC, high-resolution diffusion mapping (Hi-D) combines OF reconstruction of chromatin movements with Bayesian inference to not only quantify chromatin movements but also classify them.[158] In Hi-D, after the flow field trajectories are reconstructed by OF, motion type classification is done by using a Bayesian inference approach to evaluate the mean squared displacement (MSD) of each tracked chromatin against common models of chromatin movement.[159] This approach allows the movement of chromatin to be classified as free diffusion, subdiffusive (anomalous diffusion), directed motion, or a combination. Through Hi-D, three parameters can be calculated and used to create the reconstruction maps: the diffusion constant (D), the anomalous exponent (a), and the drift velocity (V). Maps of each parameter have shown that, in agreement with other techniques, chromatin dynamics are not uniform throughout the nucleus. Moreover, the bulk of chromatin movement may be subdiffusive while few display directed diffusion. Reconstruction maps were also be fed into computer models to identify three subpopulations of movement: slow, intermediate, and fast. These subpopulations are irrespective of D and a, while maps of V were too sparse for further analysis. A summary of the workflow and the parameter maps can be found in Figure 6B. Maps of D correlate with earlier findings, where chromatin with low mobility, thus low diffusion, remains clustered along the nuclear periphery while higher mobility, higher diffusion chromatin remains in the nuclear interior. a, the anomalous exponent which accounts for movement that cannot be definitively described as directed, reveals a similar, if less pronounced pattern. Hi-D maps can be validated using other single particle tracking methods,[160] yet provide more accurate estimations of D in dense conditions while other methods are better suited to sparser conditions.

Hi-D, along with other methods, has been used to show that transcription affects chromatin movement. However, Hi-D has gone farther and shown how transcription affects RNA polymerase II movement, creating three kinetically different groups of RNA Pol II binding.[158] Hi-D analysis has revealed that each population of RNA Pol II binding had significantly higher diffusion constants in transcriptionally active cells than in transcriptionally inactive cells. In the inactive cells, there was less quickly diffusing RNA Pol II, and when elongation was inhibited, there was an increase in the slowly diffusing RNA Pol II population. This might suggest that the mobility of RNA Pol II is dependent on the transcriptional state of the cell.

Going further than the dynamics of RNA Pol II, Hi-D, alongside DFCC, was also used to study the effects of individual transcription factors (TFs) on chromatin mobility.[161] Two TFs, CDX2 and SIX6, were chosen for their transcriptional activation and repression activities, respectively. It was found that, due to the large number of chromatin binding sites, both proteins increased chromatin mobility, but they did so with opposite effects on coherent motion. Both proteins thus led to corresponding increases in D. CDX2 led to an increase in the magnitude of directionally coordinated movements, thus changing interchromatin interactions and inducing movement of chromatin into A compartments, consistent with its activity as a transcriptional activator. Meanwhile, SIX6 led to a decrease in directionally coordinated movements over shorter lengths, consistent with earlier reports (Nozaki et al.,[78] Shaban et al.[154]). Hi-D thus presents a powerful analysis that be used to study the impact of other TFs and chromatin associated proteins on chromatin dynamics.

CONCLUSION

While conventional methods have been primarily limited to capturing static information about chromatin structure or contact, newer techniques circumvent this by providing higher resolution of imaging, using gentler sample preparation methods, and employing strategies that minimally perturb native structure/interactions. However, these newer methods can struggle with specificity for these loci, resolution, interpretation of data, etc. Although STORM provides superior resolution, the expansive instrument, massive amount of data, and requirements of sample fixation are its drawbacks. For all the versatility and various targets that CRISPR-based methods offer, it is still limited by the potential for the system to perturb native movement within live cells. STORM and CRISPR-based methods still face the remaining challenges of better resolution, integration of more colors for enhanced tracking of different genomic loci, lowering of undesired background fluorescence, and tracking of faster chromatin movements.

While the methods discussed in this review have made progress toward each challenge, CRISPR resolution, for example, is still limited by localization of sgRNAs and the fluorescence intensities of fluorescent proteins. It is also known that excitation laser light and protein fluorescence emission can be phototoxic to living systems. Tracking of faster chromatin movements, for another example, is also limited by concerns of phototoxicity and potential photobleaching of fluorophores. As discussed, movement of larger loci is a slow process but leads to larger shifts in signal localization compared to smaller loci which would be faster but with correspondingly smaller shifts in signal localization, which may be undetectable depending on the sensitivity of the camera used to record such movements. While this work has primarily focused on tracking chromatin through changes in chromatin density and organization during transcription and cell replication from a molecular biology standpoint, others have tackled the same issue from other perspectives (see Agbleke et al.,[1] Shaban et al.,[162] and Shaban et al.[163]). Going forward, advances in chromatin tracking can be used to elucidate mechanisms driving global chromatin changes, changes in response to DNA damage, effects of histone modifications on chromatin packing and distribution, etc.

AUTHOR INFORMATION

Corresponding Author

Hui-Ting Lee − *Department of Chemistry, The University of Alabama at Birmingham, Birmingham, Alabama 35294-1240, United States;* orcid.org/0000-0002-2648-4053; Email: htlee@uab.edu

https://doi.org/10.1021/cbmi.4c00033
Chem. Biomed. Imaging 2024, 2, 659−682

Author

Arianna N. Lacen − *Department of Chemistry, The University of Alabama at Birmingham, Birmingham, Alabama 35294-1240, United States;* orcid.org/0009-0008-7271-6493

Complete contact information is available at: https://pubs.acs.org/10.1021/cbmi.4c00033

Notes

The authors declare no competing financial interest.

■ ACKNOWLEDGMENTS

This review is supported by the National Science Foundation under Grant MCB-2338902.

■ VOCABULARY

chromatin = the complex of DNA and associated proteins that comprise chromosomes

immunofluorescence = a technique that utilizes fluorescently labeled primary antibodies specific to a cellular locus for imaging

nucleosome = the smallest repeating unit of chromatin, comprised of dsDNA wrapped around a histone protein complex

topologically associated domains (TADs) = regions of DNA that preferentially self-interact as opposed to making contacts with other regions of the genome

CRISPR = clustered regularly interspaced short palindromic repeats, a family of DNA sequences that can be utilized to modulate cellular immune response

■ REFERENCES

(1) Agbleke, A. A.; Amitai, A.; Buenrostro, J. D.; Chakrabarti, A.; Chu, L.; Hansen, A. S.; Koenig, K. M.; Labade, A. S.; Liu, S.; Nozaki, T.; et al. Advances in Chromatin and Chromosome Research: Perspectives from Multiple Fields. *Mol. Cell* **2020**, *79* (6), 881−901.

(2) Luger, K.; Mäder, A. W.; Richmond, R. K.; Sargent, D. F.; Richmond, T. J. Crystal structure of the nucleosome core particle at 2.8 A resolution. *Nature* **1997**, *389* (6648), 251−260.

(3) Richmond, T. J.; Finch, J. T.; Rushton, B.; Rhodes, D.; Klug, A. Structure of the nucleosome core particle at 7 A resolution. *Nature* **1984**, *311* (5986), 532−537.

(4) Li, G.; Levitus, M.; Bustamante, C.; Widom, J. Rapid spontaneous accessibility of nucleosomal DNA. *Nat. Struct Mol. Biol.* **2005**, *12* (1), 46−53.

(5) Hodges, C.; Bintu, L.; Lubkowska, L.; Kashlev, M.; Bustamante, C. Nucleosomal fluctuations govern the transcription dynamics of RNA polymerase II. *Science* **2009**, *325* (5940), 626−628.

(6) Polach, K. J.; Widom, J. Mechanism of protein access to specific DNA sequences in chromatin: a dynamic equilibrium model for gene regulation. *J. Mol. Biol.* **1995**, *254* (2), 130−149.

(7) Koopmans, W. J.; Brehm, A.; Logie, C.; Schmidt, T.; van Noort, J. Single-pair FRET microscopy reveals mononucleosome dynamics. *J. Fluoresc* **2007**, *17* (6), 785−795.

(8) Thoma, F.; Koller, T.; Klug, A. Involvement of histone H1 in the organization of the nucleosome and of the salt-dependent superstructures of chromatin. *J. Cell Biol.* **1979**, *83* (2), 403−427.

(9) Davey, C. A.; Sargent, D. F.; Luger, K.; Maeder, A. W.; Richmond, T. J. Solvent mediated interactions in the structure of the nucleosome core particle at 1.9 a resolution. *J. Mol. Biol.* **2002**, *319* (5), 1097−1113.

(10) Taverna, S. D.; Li, H.; Ruthenburg, A. J.; Allis, C. D.; Patel, D. J. How chromatin-binding modules interpret histone modifications: lessons from professional pocket pickers. *Nat. Struct Mol. Biol.* **2007**, *14* (11), 1025−1040.

(11) Martin, C.; Zhang, Y. The diverse functions of histone lysine methylation. *Nat. Rev. Mol. Cell Biol.* **2005**, *6* (11), 838−849.

(12) Grunstein, M. Histone acetylation in chromatin structure and transcription. *Nature* **1997**, *389* (6649), 349−352.

(13) Scheffer, M. P.; Eltsov, M.; Frangakis, A. S. Evidence for short-range helical order in the 30-nm chromatin fibers of erythrocyte nuclei. *Proc. Natl. Acad. Sci. U. S. A.* **2011**, *108* (41), 16992−16997.

(14) Tremethick, D. J. Higher-order structures of chromatin: the elusive 30 nm fiber. *Cell* **2007**, *128* (4), 651−654.

(15) Kizilyaprak, C.; Spehner, D.; Devys, D.; Schultz, P. In vivo chromatin organization of mouse rod photoreceptors correlates with histone modifications. *PLoS One* **2010**, *5* (6), No. e11039.

(16) Woodcock, C. L. Chromatin fibers observed in situ in frozen hydrated sections. Native fiber diameter is not correlated with nucleosome repeat length. *J. Cell Biol.* **1994**, *125* (1), 11−19.

(17) Finch, J. T.; Klug, A. Solenoidal model for superstructure in chromatin. *Proc. Natl. Acad. Sci. U. S. A.* **1976**, *73* (6), 1897−1901.

(18) Bustamante, C.; Zuccheri, G.; Leuba, S. H.; Yang, G.; Samori, B. Visualization and Analysis of Chromatin by Scanning Force Microscopy. *Methods* **1997**, *12* (1), 73−83.

(19) Sugiyama, S.; Yoshino, T.; Kanahara, H.; Kobori, T.; Ohtani, T. Atomic force microscopic imaging of 30 nm chromatin fiber from partially relaxed plant chromosomes. *Scanning* **2003**, *25* (3), 132−136.

(20) Ricci, M. A.; Manzo, C.; García-Parajo, M. F.; Lakadamyali, M.; Cosma, M. P. Chromatin Fibers Are Formed by Heterogeneous Groups of Nucleosomes In Vivo. *Cell* **2015**, *160* (6), 1145−1158.

(21) Kim, T. H.; Dekker, J. 3C-Based Chromatin Interaction Analyses. *Cold Spring Harb Protoc* **2018**, *2018* (9), 685.

(22) Loviglio, M. N.; Leleu, M.; Männik, K.; Passeggeri, M.; Giannuzzi, G.; van der Werf, I.; Waszak, S. M.; Zazhytska, M.; Roberts-Caldeira, I.; Gheldof, N.; et al. Chromosomal contacts connect loci associated with autism, BMI and head circumference phenotypes. *Mol. Psychiatry* **2017**, *22* (6), 836−849.

(23) van Staalduinen, J.; van Staveren, T.; Grosveld, F.; Wendt, K. S. Live-cell imaging of chromatin contacts opens a new window into chromatin dynamics. *Epigenetics & Chromatin* **2023**, *16* (1), 27.

(24) Hoffman, E. A.; Frey, B. L.; Smith, L. M.; Auble, D. T. Formaldehyde crosslinking: a tool for the study of chromatin complexes. *J. Biol. Chem.* **2015**, *290* (44), 26404−26411.

(25) Belton, J. M.; Dekker, J. Chromosome Conformation Capture (3C) in Budding Yeast. *Cold Spring Harb Protoc* **2015**, *2015* (6), 580−586.

(26) Dostie, J.; Richmond, T. A.; Arnaout, R. A.; Selzer, R. R.; Lee, W. L.; Honan, T. A.; Rubio, E. D.; Krumm, A.; Lamb, J.; Nusbaum, C.; et al. Chromosome Conformation Capture Carbon Copy (5C): a massively parallel solution for mapping interactions between genomic elements. *Genome Res.* **2006**, *16* (10), 1299−1309.

(27) Nora, E. P.; Lajoie, B. R.; Schulz, E. G.; Giorgetti, L.; Okamoto, I.; Servant, N.; Piolot, T.; van Berkum, N. L.; Meisig, J.; Sedat, J.; et al. Spatial partitioning of the regulatory landscape of the X-inactivation centre. *Nature* **2012**, *485* (7398), 381−385.

(28) Lieberman-Aiden, E.; van Berkum, N. L.; Williams, L.; Imakaev, M.; Ragoczy, T.; Telling, A.; Amit, I.; Lajoie, B. R.; Sabo, P. J.; Dorschner, M. O.; et al. Comprehensive mapping of long-range interactions reveals folding principles of the human genome. *Science* **2009**, *326* (5950), 289−293.

(29) Fortin, J. P.; Hansen, K. D. Reconstructing A/B compartments as revealed by Hi-C using long-range correlations in epigenetic data. *Genome Biol.* **2015**, *16* (1), 180.

(30) Stevens, T. J.; Lando, D.; Basu, S.; Atkinson, L. P.; Cao, Y.; Lee, S. F.; Leeb, M.; Wohlfahrt, K. J.; Boucher, W.; O'Shaughnessy-Kirwan, A.; et al. 3D structures of individual mammalian genomes studied by single-cell Hi-C. *Nature* **2017**, *544* (7648), 59−64.

(31) Lichter, P.; Cremer, T.; Borden, J.; Manuelidis, L.; Ward, D. C. Delineation of individual human chromosomes in metaphase and interphase cells by in situ suppression hybridization using recombinant DNA libraries. *Hum. Genet.* **1988**, *80* (3), 224−234.

(32) Batani, G.; Bayer, K.; Böge, J.; Hentschel, U.; Thomas, T. Fluorescence in situ hybridization (FISH) and cell sorting of living bacteria. *Sci. Rep.* **2019**, *9* (1), 18618.
(33) Young, A. P.; Jackson, D. J.; Wyeth, R. C. A technical review and guide to RNA fluorescence in situ hybridization. *PeerJ.* **2020**, *8*, No. e8806.
(34) Anton, T.; Bultmann, S.; Leonhardt, H.; Markaki, Y. Visualization of specific DNA sequences in living mouse embryonic stem cells with a programmable fluorescent CRISPR/Cas system. *Nucleus* **2014**, *5* (2), 163−172.
(35) Im, K.; Mareninov, S.; Diaz, M. F. P.; Yong, W. H. An Introduction to Performing Immunofluorescence Staining. *Methods Mol. Biol.* **2019**, *1897*, 299−311.
(36) Montpetit, A. J.; Alhareeri, A. A.; Montpetit, M.; Starkweather, A. R.; Elmore, L. W.; Filler, K.; Mohanraj, L.; Burton, C. W.; Menzies, V. S.; Lyon, D. E.; Jackson-Cook, C. K. Telomere length: a review of methods for measurement. *Nurs Res.* **2014**, *63* (4), 289−299.
(37) Nordfjäll, K.; Larefalk, A.; Lindgren, P.; Holmberg, D.; Roos, G. Telomere length and heredity: Indications of paternal inheritance. *Proc. Natl. Acad. Sci. U. S. A.* **2005**, *102* (45), 16374−16378.
(38) Srinivas, N.; Rachakonda, S.; Kumar, R. Telomeres and Telomere Length: A General Overview. *Cancers (Basel)* **2020**, *12* (3), 558.
(39) Canela, A.; Vera, E.; Klatt, P.; Blasco, M. A. High-throughput telomere length quantification by FISH and its application to human population studies. *Proc. Natl. Acad. Sci. U. S. A.* **2007**, *104* (13), 5300−5305.
(40) Röth, A.; Yssel, H.; Pène, J. r. m.; Chavez, E. A.; Schertzer, M.; Lansdorp, P. M.; Spits, H.; Luiten, R. M. Telomerase levels control the lifespan of human T lymphocytes. *Blood* **2003**, *102* (3), 849−857.
(41) Cho, N. W.; Dilley, R. L.; Lampson, M. A.; Greenberg, R. A. Interchromosomal homology searches drive directional ALT telomere movement and synapsis. *Cell* **2014**, *159* (1), 108−121.
(42) Markaki, Y.; Smeets, D.; Fiedler, S.; Schmid, V. J.; Schermelleh, L.; Cremer, T.; Cremer, M. The potential of 3D-FISH and super-resolution structured illumination microscopy for studies of 3D nuclear architecture: 3D structured illumination microscopy of defined chromosomal structures visualized by 3D (immuno)-FISH opens new perspectives for studies of nuclear architecture. *Bioessays* **2012**, *34* (5), 412−426.
(43) Brown, J. M.; Roberts, N. A.; Graham, B.; Waithe, D.; Lagerholm, C.; Telenius, J. M.; De Ornellas, S.; Oudelaar, A. M.; Scott, C.; Szczerbal, I.; et al. A tissue-specific self-interacting chromatin domain forms independently of enhancer-promoter interactions. *Nat. Commun.* **2018**, *9* (1), 3849.
(44) Winkler, R.; Perner, B.; Rapp, A.; Durm, M.; Cremer, C.; Greulich, K. O.; Hausmann, M. Labelling quality and chromosome morphology after low temperature FISH analysed by scanning far-field and near-field optical microscopy. *J. Microsc* **2003**, *209* (1), 23−33.
(45) Wang, Y.; Cottle, W. T.; Wang, H.; Feng, X. A.; Mallon, J.; Gavrilov, M.; Bailey, S.; Ha, T. Genome oligopaint via local denaturation fluorescence in situ hybridization. *Mol. Cell* **2021**, *81* (7), 1566−1577.
(46) Knauert, M. P.; Glazer, P. M. Triplex forming oligonucleotides: sequence-specific tools for gene targeting. *Hum. Mol. Genet.* **2001**, *10* (20), 2243−2251.
(47) Goni, J. R.; de la Cruz, X.; Orozco, M. Triplex-forming oligonucleotide target sequences in the human genome. *Nucleic Acids Res.* **2004**, *32* (1), 354−360.
(48) Pradhan, S.; Apaydin, S.; Bucevicius, J.; Gerasimaite, R.; Kostiuk, G.; Lukinavicius, G. Sequence-specific DNA labelling for fluorescence microscopy. *Biosens Bioelectron* **2023**, *230*, 115256.
(49) Frank-Kamenetskii, M. D.; Mirkin, S. M. Triplex DNA structures. *Annu. Rev. Biochem.* **1995**, *64*, 65−95.
(50) Lee, J. S.; Johnson, D. A.; Morgan, A. R. Complexes formed by (pyrimidine)n. (purine)n DNAs on lowering the pH are three-stranded. *Nucleic Acids Res.* **1979**, *6* (9), 3073−3091.
(51) Li, C.; Zhou, Z.; Ren, C.; Deng, Y.; Peng, F.; Wang, Q.; Zhang, H.; Jiang, Y. Triplex-forming oligonucleotides as an anti-gene technique for cancer therapy. *Front Pharmacol* **2022**, *13*, 1007723.
(52) Vekhoff, P.; Ceccaldi, A.; Polverari, D.; Pylouster, J.; Pisano, C.; Arimondo, P. B. Triplex formation on DNA targets: how to choose the oligonucleotide. *Biochemistry* **2008**, *47* (47), 12277−12289.
(53) Lee, J.-H.; Tchetgna, F. L. D.; Cremer, C.; Bestvater, F.; Schmitt, E.; Hausmann, M.; Krufzik, M. COMBO-FISH: A Versatile Tool Beyond Standard FISH to Study Chromatin Organization by Fluorescence Light Microscopy. *OBM Genetics* **2019**, *3* (1), 064.
(54) Elliott, A. D. Confocal Microscopy: Principles and Modern Practices. *Curr. Protoc Cytom* **2020**, *92* (1), No. e68.
(55) St. Croix, C. M.; Shand, S. H.; Watkins, S. C. Confocal microscopy: comparisons, applications, and problems. *Biotechniques* **2005**, *39* (sup6), S2−S5.
(56) Xu, J.; Ma, H.; Liu, Y. Stochastic Optical Reconstruction Microscopy (STORM). *Curr Protoc Cytom* **2017**, *81*, 12.46.1−12.46.27.
(57) Rust, M. J.; Bates, M.; Zhuang, X. Sub-diffraction-limit imaging by stochastic optical reconstruction microscopy (STORM). *Nat. Methods* **2006**, *3* (10), 793−795.
(58) Boettiger, A. N.; Bintu, B.; Moffitt, J. R.; Wang, S.; Beliveau, B. J.; Fudenberg, G.; Imakaev, M.; Mirny, L. A.; Wu, C. T.; Zhuang, X. Super-resolution imaging reveals distinct chromatin folding for different epigenetic states. *Nature* **2016**, *529* (7586), 418−422.
(59) Boettiger, A.; Murphy, S. Advances in Chromatin Imaging at Kilobase-Scale Resolution. *Trends Genet* **2020**, *36* (4), 273−287.
(60) Bates, M.; Huang, B.; Dempsey, G. T.; Zhuang, X. Multicolor super-resolution imaging with photo-switchable fluorescent probes. *Science* **2007**, *317* (5845), 1749−1753.
(61) Xu, J.; Ma, H.; Jin, J.; Uttam, S.; Fu, R.; Huang, Y.; Liu, Y. Super-Resolution Imaging of Higher-Order Chromatin Structures at Different Epigenomic States in Single Mammalian Cells. *Cell Rep* **2018**, *24* (4), 873−882.
(62) Beliveau, B. J.; Apostolopoulos, N.; Wu, C. T. Visualizing genomes with Oligopaint FISH probes. *Curr. Protoc. Mol. Biol.* **2014**, *105*, 14.23.1−14.23.20.
(63) Beliveau, B. J.; Boettiger, A. N.; Avendaño, M. S.; Jungmann, R.; McCole, R. B.; Joyce, E. F.; Kim-Kiselak, C.; Bantignies, F.; Fonseka, C. Y.; Erceg, J.; et al. Single-molecule super-resolution imaging of chromosomes and in situ haplotype visualization using Oligopaint FISH probes. *Nat. Commun.* **2015**, *6* (1), 7147.
(64) Beliveau, B. J.; Boettiger, A. N.; Nir, G.; Bintu, B.; Yin, P.; Zhuang, X.; Wu, C. T. In Situ Super-Resolution Imaging of Genomic DNA with OligoSTORM and OligoDNA-PAINT. *Methods Mol. Biol.* **2017**, *1663*, 231−252.
(65) Bintu, B.; Mateo, L. J.; Su, J. H.; Sinnott-Armstrong, N. A.; Parker, M.; Kinrot, S.; Yamaya, K.; Boettiger, A. N.; Zhuang, X. Super-resolution chromatin tracing reveals domains and cooperative interactions in single cells. *Science* **2018**, *362* (6413), eaau1783.
(66) Kearney, L. Multiplex-FISH (M-FISH): technique, developments and applications. *Cytogenetic and Genome Research* **2006**, *114*, 189−198.
(67) Guelen, L.; Pagie, L.; Brasset, E.; Meuleman, W.; Faza, M. B.; Talhout, W.; Eussen, B. H.; de Klein, A.; Wessels, L.; de Laat, W.; van Steensel, B. Domain organization of human chromosomes revealed by mapping of nuclear lamina interactions. *Nature* **2008**, *453* (7197), 948−951.
(68) Xu, J.; Ma, H.; Ma, H.; Jiang, W.; Mela, C. A.; Duan, M.; Zhao, S.; Gao, C.; Hahm, E.-R.; Lardo, S. M.; et al. Super-resolution imaging reveals the evolution of higher-order chromatin folding in early carcinogenesis. *Nat. Commun.* **2020**, *11* (1), 1899.
(69) Tóth, K. F.; Knoch, T. A.; Wachsmuth, M.; Frank-Stöhr, M.; Stöhr, M.; Bacher, C. P.; Müller, G.; Rippe, K. Trichostatin A-induced histone acetylation causes decondensation of interphase chromatin. *Journal of cell science* **2004**, *117* (18), 4277−4287.
(70) Manley, S.; Gillette, J. M.; Patterson, G. H.; Shroff, H.; Hess, H. F.; Betzig, E.; Lippincott-Schwartz, J. High-density mapping of single-

molecule trajectories with photoactivated localization microscopy. *Nat. Methods* **2008**, *5* (2), 155−157.
(71) Shroff, H.; Galbraith, C. G.; Galbraith, J. A.; Betzig, E. Live-cell photoactivated localization microscopy of nanoscale adhesion dynamics. *Nat. Methods* **2008**, *5* (5), 417−423.
(72) Greenfield, D.; McEvoy, A. L.; Shroff, H.; Crooks, G. E.; Wingreen, N. S.; Betzig, E.; Liphardt, J. Self-organization of the Escherichia coli chemotaxis network imaged with super-resolution light microscopy. *PLoS Biol.* **2009**, *7* (6), No. e1000137.
(73) Lee, S. H.; Shin, J. Y.; Lee, A.; Bustamante, C. Counting single photoactivatable fluorescent molecules by photoactivated localization microscopy (PALM). *Proc. Natl. Acad. Sci. U. S. A.* **2012**, *109* (43), 17436−17441.
(74) Annibale, P.; Vanni, S.; Scarselli, M.; Rothlisberger, U.; Radenovic, A. Quantitative photo activated localization microscopy: unraveling the effects of photoblinking. *PLoS One* **2011**, *6* (7), No. e22678.
(75) Liu, C.; Yuen, J.; Torralba, A. SIFT flow: dense correspondence across scenes and its applications. *IEEE Trans Pattern Anal Mach Intell* **2011**, *33* (5), 978−994.
(76) Nehme, E.; Weiss, L. E.; Michaeli, T.; Shechtman, Y. Deep-STORM: super-resolution single-molecule microscopy by deep learning. *Optica* **2018**, *5* (4), 458−464.
(77) Barth, R.; Bystricky, K.; Shaban, H. A. Coupling chromatin structure and dynamics by live super-resolution imaging. *Sci. Adv.* **2020**, *6* (27), eaaz2196.
(78) Nozaki, T.; Imai, R.; Tanbo, M.; Nagashima, R.; Tamura, S.; Tani, T.; Joti, Y.; Tomita, M.; Hibino, K.; Kanemaki, M. T.; et al. Dynamic Organization of Chromatin Domains Revealed by Super-Resolution Live-Cell Imaging. *Mol. Cell* **2017**, *67* (2), 282−293.
(79) Barth, R.; Fourel, G.; Shaban, H. A. Dynamics as a cause for the nanoscale organization of the genome. *Nucleus* **2020**, *11* (1), 83−98.
(80) Granger, C. W. J. Investigating Causal Relations by Econometric Models and Cross-spectral Methods. *Econometrica* **1969**, *37* (3), 424−438.
(81) Doguwa, S. I. On the estimation of the point-object nearest neighbour distribution F(y) for point processes. *Journal of Statistical Computation and Simulation* **1992**, *41* (1−2), 95−107.
(82) Datta, R.; Heaster, T. M.; Sharick, J. T.; Gillette, A. A.; Skala, M. C. Fluorescence lifetime imaging microscopy: fundamentals and advances in instrumentation, analysis, and applications. *J. Biomed Opt* **2020**, *25* (7), 1−43.
(83) Sekar, R. B.; Periasamy, A. Fluorescence resonance energy transfer (FRET) microscopy imaging of live cell protein localizations. *J. Cell Biol.* **2003**, *160* (5), 629−633.
(84) Zheng, J. Spectroscopy-based quantitative fluorescence resonance energy transfer analysis. *Methods Mol. Biol.* **2006**, *337*, 65−77.
(85) Schneckenburger, H. Forster resonance energy transfer-what can we learn and how can we use it? *Methods Appl. Fluoresc* **2020**, *8* (1), 013001.
(86) Clegg, R. M. Chapter 1 Förster resonance energy transfer—FRET what is it, why do it, and how it's done. *Laboratory Techniques in Biochemistry and Molecular Biology* **2009**, *33*, 1−57.
(87) Liput, D. J.; Nguyen, T. A.; Augustin, S. M.; Lee, J. O.; Vogel, S. S. A Guide to Fluorescence Lifetime Microscopy and Forster's Resonance Energy Transfer in Neuroscience. *Curr. Protoc Neurosci* **2020**, *94* (1), No. e108.
(88) Lleres, D.; Bailly, A. P.; Perrin, A.; Norman, D. G.; Xirodimas, D. P.; Feil, R. Quantitative FLIM-FRET Microscopy to Monitor Nanoscale Chromatin Compaction In Vivo Reveals Structural Roles of Condensin Complexes. *Cell Rep* **2017**, *18* (7), 1791−1803.
(89) Lui, D. Y.; Colaiacovo, M. P. Meiotic development in Caenorhabditis elegans. *Adv. Exp. Med. Biol.* **2013**, *757*, 133−170.
(90) Gustafsson, M. G. Surpassing the lateral resolution limit by a factor of two using structured illumination microscopy. *J. Microsc* **2000**, *198* (2), 82−87.
(91) Engelhardt, K.; Häusler, G. Acquisition of 3-D data by focus sensing. *Applied optics* **1988**, *27* (22), 4684−4689.
(92) Heintzmann, R.; Huser, T. Super-Resolution Structured Illumination Microscopy. *Chem. Rev.* **2017**, *117* (23), 13890−13908.
(93) Frohn, J. T.; Knapp, H. F.; Stemmer, A. True optical resolution beyond the Rayleigh limit achieved by standing wave illumination. *Proc. Natl. Acad. Sci. U. S. A.* **2000**, *97* (13), 7232−7236.
(94) So, P. T.; Kwon, H.-S.; Dong, C. Y. Resolution enhancement in standing-wave total internal reflection microscopy: a point-spread-function engineering approach. *JOSA A* **2001**, *18* (11), 2833−2845.
(95) Miron, E.; Oldenkamp, R.; Brown, J. M.; Pinto, D. M. S.; Xu, C. S.; Faria, A. R.; Shaban, H. A.; Rhodes, J. D. P.; Innocent, C.; de Ornellas, S.; et al. Chromatin arranges in chains of mesoscale domains with nanoscale functional topography independent of cohesin. *Science Advances* **2020**, *6* (39), No. eaba8811.
(96) Markaki, Y.; Gunkel, M.; Schermelleh, L.; Beichmanis, S.; Neumann, J.; Heidemann, M.; Leonhardt, H.; Eick, D.; Cremer, C.; Cremer, T. Functional nuclear organization of transcription and DNA replication: a topographical marriage between chromatin domains and the interchromatin compartment. *Cold Spring Harb Symp. Quant Biol.* **2010**, *75*, 475−492.
(97) Schermelleh, L.; Carlton, P. M.; Haase, S.; Shao, L.; Winoto, L.; Kner, P.; Burke, B.; Cardoso, M. C.; Agard, D. A.; Gustafsson, M. G.; et al. Subdiffraction multicolor imaging of the nuclear periphery with 3D structured illumination microscopy. *Science* **2008**, *320* (5881), 1332−1336.
(98) Smeets, D.; Markaki, Y.; Schmid, V. J.; Kraus, F.; Tattermusch, A.; Cerase, A.; Sterr, M.; Fiedler, S.; Demmerle, J.; Popken, J.; et al. Three-dimensional super-resolution microscopy of the inactive X chromosome territory reveals a collapse of its active nuclear compartment harboring distinct Xist RNA foci. *Epigenetics & Chromatin* **2014**, *7* (1), 8.
(99) Bruinsma, R.; Grosberg, A. Y.; Rabin, Y.; Zidovska, A. Chromatin hydrodynamics. *Biophys. J.* **2014**, *106* (9), 1871−1881.
(100) Jinek, M.; Chylinski, K.; Fonfara, I.; Hauer, M.; Doudna, J. A.; Charpentier, E. A programmable dual-RNA-guided DNA endonuclease in adaptive bacterial immunity. *Science* **2012**, *337* (6096), 816−821.
(101) Gleditzsch, D.; Pausch, P.; Müller-Esparza, H.; Özcan, A.; Guo, X.; Bange, G.; Randau, L. PAM identification by CRISPR-Cas effector complexes: diversified mechanisms and structures. *RNA Biol.* **2019**, *16* (4), 504−517.
(102) Tian, M.; Zhang, R.; Li, J. Emergence of CRISPR/Cas9-mediated bioimaging: A new dawn of in-situ detection. *Biosens. Bioelectron.* **2023**, *232*, 115302.
(103) Knight, S. C.; Tjian, R.; Doudna, J. A. Genomes in Focus: Development and Applications of CRISPR-Cas9 Imaging Technologies. *Angew. Chem., Int. Ed.* **2018**, *57* (16), 4329−4337.
(104) Qin, P.; Parlak, M.; Kuscu, C.; Bandaria, J.; Mir, M.; Szlachta, K.; Singh, R.; Darzacq, X.; Yildiz, A.; Adli, M. Live cell imaging of low- and non-repetitive chromosome loci using CRISPR-Cas9. *Nat. Commun.* **2017**, *8*, 14725.
(105) Bronshtein, I.; Kepten, E.; Kanter, I.; Berezin, S.; Lindner, M.; Redwood, A. B.; Mai, S.; Gonzalo, S.; Foisner, R.; Shav-Tal, Y.; Garini, Y. Loss of lamin A function increases chromatin dynamics in the nuclear interior. *Nat. Commun.* **2015**, *6*, 8044.
(106) Marshall, W. F.; Straight, A.; Marko, J. F.; Swedlow, J.; Dernburg, A.; Belmont, A.; Murray, A. W.; Agard, D. A.; Sedat, J. W. Interphase chromosomes undergo constrained diffusional motion in living cells. *Curr. Biol.* **1997**, *7* (12), 930−939.
(107) Molenaar, C.; Wiesmeijer, K.; Verwoerd, N. P.; Khazen, S.; Eils, R.; Tanke, H. J.; Dirks, R. W. Visualizing telomere dynamics in living mammalian cells using PNA probes. *Embo j* **2003**, *22* (24), 6631−6641.
(108) Bancaud, A.; Huet, S.; Daigle, N.; Mozziconacci, J.; Beaudouin, J.; Ellenberg, J. Molecular crowding affects diffusion and binding of nuclear proteins in heterochromatin and reveals the fractal organization of chromatin. *Embo j* **2009**, *28* (24), 3785−3798.
(109) Wang, X.; Kam, Z.; Carlton, P. M.; Xu, L.; Sedat, J. W.; Blackburn, E. H. Rapid telomere motions in live human cells analyzed

https://doi.org/10.1021/cbmi.4c00033
Chem. Biomed. Imaging 2024, 2, 659−682

by highly time-resolved microscopy. *Epigenetics Chromatin* **2008**, *1* (1), 4.
(110) Dimitrova, N.; Chen, Y. C.; Spector, D. L.; de Lange, T. 53BP1 promotes non-homologous end joining of telomeres by increasing chromatin mobility. *Nature* **2008**, *456* (7221), 524−528.
(111) Chen, B.; Gilbert, L. A.; Cimini, B. A.; Schnitzbauer, J.; Zhang, W.; Li, G. W.; Park, J.; Blackburn, E. H.; Weissman, J. S.; Qi, L. S.; Huang, B. Dynamic imaging of genomic loci in living human cells by an optimized CRISPR/Cas system. *Cell* **2013**, *155* (7), 1479−1491.
(112) Shao, S.; Zhang, W.; Hu, H.; Xue, B.; Qin, J.; Sun, C.; Sun, Y.; Wei, W.; Sun, Y. Long-term dual-color tracking of genomic loci by modified sgRNAs of the CRISPR/Cas9 system. *Nucleic Acids Res.* **2016**, *44* (9), No. e86.
(113) Ma, H.; Naseri, A.; Reyes-Gutierrez, P.; Wolfe, S. A.; Zhang, S.; Pederson, T. Multicolor CRISPR labeling of chromosomal loci in human cells. *Proc. Natl. Acad. Sci. U. S. A.* **2015**, *112* (10), 3002−3007.
(114) Fu, Y.; Rocha, P. P.; Luo, V. M.; Raviram, R.; Deng, Y.; Mazzoni, E. O.; Skok, J. A. CRISPR-dCas9 and sgRNA scaffolds enable dual-colour live imaging of satellite sequences and repeat-enriched individual loci. *Nat. Commun.* **2016**, *7* (1), 11707.
(115) Romei, M. G.; Boxer, S. G. Split Green Fluorescent Proteins: Scope, Limitations, and Outlook. *Annu. Rev. Biophys* **2019**, *48*, 19−44.
(116) Tanenbaum, M. E.; Gilbert, L. A.; Qi, L. S.; Weissman, J. S.; Vale, R. D. A protein-tagging system for signal amplification in gene expression and fluorescence imaging. *Cell* **2014**, *159* (3), 635−646.
(117) Chaudhary, N.; Nho, S.-H.; Cho, H.; Gantumur, N.; Ra, J. S.; Myung, K.; Kim, H. Background-suppressed live visualization of genomic loci with an improved CRISPR system based on a split fluorophore. *Genome Res.* **2020**, *30* (9), 1306−1316.
(118) Fioriniello, S.; Marano, D.; Fiorillo, F.; D'Esposito, M.; Della Ragione, F. Epigenetic Factors That Control Pericentric Heterochromatin Organization in Mammals. *Genes (Basel)* **2020**, *11* (6), 595.
(119) Mayer, R.; Brero, A.; von Hase, J.; Schroeder, T.; Cremer, T.; Dietzel, S. Common themes and cell type specific variations of higher order chromatin arrangements in the mouse. *BMC Cell Biol.* **2005**, *6*, 44.
(120) Della Ragione, F.; Vacca, M.; Fioriniello, S.; Pepe, G.; D'Esposito, M. MECP2, a multi-talented modulator of chromatin architecture. *Brief Funct Genomics* **2016**, *15* (6), 420−431.
(121) Probst, A. V.; Almouzni, G. Pericentric heterochromatin: dynamic organization during early development in mammals. *Differentiation* **2008**, *76* (1), 15−23.
(122) Kipling, D.; Ackford, H. E.; Taylor, B. A.; Cooke, H. J. Mouse minor satellite DNA genetically maps to the centromere and is physically linked to the proximal telomere. *Genomics* **1991**, *11* (2), 235−241.
(123) Clow, P. A.; Du, M.; Jillette, N.; Taghbalout, A.; Zhu, J. J.; Cheng, A. W. CRISPR-mediated multiplexed live cell imaging of nonrepetitive genomic loci with one guide RNA per locus. *Nat. Commun.* **2022**, *13* (1), 1871.
(124) Rao, S. S. P.; Huang, S. C.; Glenn St Hilaire, B.; Engreitz, J. M.; Perez, E. M.; Kieffer-Kwon, K. R.; Sanborn, A. L.; Johnstone, S. E.; Bascom, G. D.; Bochkov, I. D.; et al. Cohesin Loss Eliminates All Loop Domains. *Cell* **2017**, *171* (2), 305−320.
(125) Gassler, J.; Brandão, H. B.; Imakaev, M.; Flyamer, I. M.; Ladstätter, S.; Bickmore, W. A.; Peters, J. M.; Mirny, L. A.; Tachibana, K. A mechanism of cohesin-dependent loop extrusion organizes zygotic genome architecture. *Embo j* **2017**, *36* (24), 3600−3618.
(126) Lyu, X.-Y.; Deng, Y.; Huang, X.-Y.; Li, Z.-Z.; Fang, G.-Q.; Yang, D.; Wang, F.-L.; Kang, W.; Shen, E.-Z.; Song, C.-Q. CRISPR FISHer enables high-sensitivity imaging of nonrepetitive DNA in living cells through phase separation-mediated signal amplification. *Cell Research* **2022**, *32* (11), 969−981.
(127) Meier, S.; Güthe, S.; Kiefhaber, T.; Grzesiek, S. Foldon, the natural trimerization domain of T4 fibritin, dissociates into a monomeric A-state form containing a stable beta-hairpin: atomic details of trimer dissociation and local beta-hairpin stability from residual dipolar couplings. *J. Mol. Biol.* **2004**, *344* (4), 1051−1069.
(128) Güthe, S.; Kapinos, L.; Möglich, A.; Meier, S.; Grzesiek, S.; Kiefhaber, T. Very fast folding and association of a trimerization domain from bacteriophage T4 fibritin. *J. Mol. Biol.* **2004**, *337* (4), 905−915.
(129) Ling, X.; Han, Y.; Meng, J.; Zhong, B.; Chen, J.; Zhang, H.; Qin, J.; Pang, J.; Liu, L. Small extrachromosomal circular DNA (eccDNA): major functions in evolution and cancer. *Molecular Cancer* **2021**, *20* (1), 113.
(130) Yang, L.; Jia, R.; Ge, T.; Ge, S.; Zhuang, A.; Chai, P.; Fan, X. Extrachromosomal circular DNA: biogenesis, structure, functions and diseases. *Signal Transduct Target Ther* **2022**, *7* (1), 342.
(131) Zuo, S.; Yi, Y.; Wang, C.; Li, X.; Zhou, M.; Peng, Q.; Zhou, J.; Yang, Y.; He, Q. Extrachromosomal Circular DNA (eccDNA): From Chaos to Function. *Frontiers in Cell and Developmental Biology* **2022**, *9*, 792555.
(132) Gaj, T.; Gersbach, C. A.; Barbas, C. F., 3rd ZFN, TALEN, and CRISPR/Cas-based methods for genome engineering. *Trends Biotechnol* **2013**, *31* (7), 397−405.
(133) Moscou, M. J.; Bogdanove, A. J. A simple cipher governs DNA recognition by TAL effectors. *Science* **2009**, *326* (5959), 1501.
(134) Boch, J.; Scholze, H.; Schornack, S.; Landgraf, A.; Hahn, S.; Kay, S.; Lahaye, T.; Nickstadt, A.; Bonas, U. Breaking the code of DNA binding specificity of TAL-type III effectors. *Science* **2009**, *326* (5959), 1509−1512.
(135) Miller, J. C.; Tan, S.; Qiao, G.; Barlow, K. A.; Wang, J.; Xia, D. F.; Meng, X.; Paschon, D. E.; Leung, E.; Hinkley, S. J.; et al. A TALE nuclease architecture for efficient genome editing. *Nat. Biotechnol.* **2011**, *29* (2), 143−148.
(136) Christian, M.; Cermak, T.; Doyle, E. L.; Schmidt, C.; Zhang, F.; Hummel, A.; Bogdanove, A. J.; Voytas, D. F. Targeting DNA double-strand breaks with TAL effector nucleases. *Genetics* **2010**, *186* (2), 757−761.
(137) Miyanari, Y.; Ziegler-Birling, C.; Torres-Padilla, M.-E. Live visualization of chromatin dynamics with fluorescent TALEs. *Nature Structural & Molecular Biology* **2013**, *20* (11), 1321−1324.
(138) Thanisch, K.; Schneider, K.; Morbitzer, R.; Solovei, I.; Lahaye, T.; Bultmann, S.; Leonhardt, H. Targeting and tracing of specific DNA sequences with dTALEs in living cells. *Nucleic Acids Res.* **2014**, *42* (6), No. e38.
(139) Lippincott-Schwartz, J.; Snapp, E. L.; Phair, R. D. The Development and Enhancement of FRAP as a Key Tool for Investigating Protein Dynamics. *Biophys. J.* **2018**, *115* (7), 1146−1155.
(140) Phair, R. D.; Misteli, T. Kinetic modelling approaches to in vivo imaging. *Nat. Rev. Mol. Cell Biol.* **2001**, *2* (12), 898−907.
(141) Ma, H.; Reyes-Gutierrez, P.; Pederson, T. Visualization of repetitive DNA sequences in human chromosomes with transcription activator-like effectors. *Proc. Natl. Acad. Sci. U. S. A.* **2013**, *110* (52), 21048−21053.
(142) Li, Y.; Almassalha, L. M.; Chandler, J. E.; Zhou, X.; Stypula-Cyrus, Y. E.; Hujsak, K. A.; Roth, E. W.; Bleher, R.; Subramanian, H.; Szleifer, I.; et al. The effects of chemical fixation on the cellular nanostructure. *Exp. Cell Res.* **2017**, *358* (2), 253−259.
(143) Hihara, S.; Pack, C. G.; Kaizu, K.; Tani, T.; Hanafusa, T.; Nozaki, T.; Takemoto, S.; Yoshimi, T.; Yokota, H.; Imamoto, N.; et al. Local nucleosome dynamics facilitate chromatin accessibility in living mammalian cells. *Cell Rep* **2012**, *2* (6), 1645−1656.
(144) Lemaitre, C.; Bickmore, W. A. Chromatin at the nuclear periphery and the regulation of genome functions. *Histochem Cell Biol.* **2015**, *144* (2), 111−122.
(145) Ryba, T.; Hiratani, I.; Lu, J.; Itoh, M.; Kulik, M.; Zhang, J.; Schulz, T. C.; Robins, A. J.; Dalton, S.; Gilbert, D. M. Evolutionarily conserved replication timing profiles predict long-range chromatin interactions and distinguish closely related cell types. *Genome Res.* **2010**, *20* (6), 761−770.

https://doi.org/10.1021/cbmi.4c00033
Chem. Biomed. Imaging 2024, 2, 659−682

(146) Meshorer, E.; Misteli, T. Chromatin in pluripotent embryonic stem cells and differentiation. *Nat. Rev. Mol. Cell Biol.* **2006**, *7* (7), 540−546.
(147) Lerner, J.; Gomez-Garcia, P. A.; McCarthy, R. L.; Liu, Z.; Lakadamyali, M.; Zaret, K. S. Two-Parameter Mobility Assessments Discriminate Diverse Regulatory Factor Behaviors in Chromatin. *Mol. Cell* **2020**, *79* (4), 677−688.
(148) Wieser, S.; Schutz, G. J. Tracking single molecules in the live cell plasma membrane-Do's and Don't's. *Methods* **2008**, *46* (2), 131−140.
(149) van Steensel, B.; Belmont, A. S. Lamina-Associated Domains: Links with Chromosome Architecture, Heterochromatin, and Gene Repression. *Cell* **2017**, *169* (5), 780−791.
(150) Vig, D. K.; Hamby, A. E.; Wolgemuth, C. W. On the Quantification of Cellular Velocity Fields. *Biophys. J.* **2016**, *110* (7), 1469−1475.
(151) Horn, B. K. P.; Schunck, B. G. Determining optical flow. *Artificial Intelligence* **1981**, *17* (1), 185−203.
(152) Sveen, J. K. An Introduction to MatPIV v.1.6.1. *Preprint Series. Mechanics and Applied Mathematics*, 2004. http://urn.nb.no/URN:NBN:no-27806.
(153) Gautama, T.; Van Hulle, M. A. A phase-based approach to the estimation of the optical flow field using spatial filtering. *IEEE Trans Neural Netw* **2002**, *13* (5), 1127−1136.
(154) Shaban, H. A.; Barth, R.; Bystricky, K. Formation of correlated chromatin domains at nanoscale dynamic resolution during transcription. *Nucleic Acids Res.* **2018**, *46* (13), No. e77.
(155) Germier, T.; Kocanova, S.; Walther, N.; Bancaud, A.; Shaban, H. A.; Sellou, H.; Politi, A. Z.; Ellenberg, J.; Gallardo, F.; Bystricky, K. Real-Time Imaging of a Single Gene Reveals Transcription-Initiated Local Confinement. *Biophys. J.* **2017**, *113* (7), 1383−1394.
(156) Hozak, P.; Hassan, A. B.; Jackson, D. A.; Cook, P. R. Visualization of replication factories attached to nucleoskeleton. *Cell* **1993**, *73* (2), 361−373.
(157) Zidovska, A.; Weitz, D. A.; Mitchison, T. J. Micron-scale coherence in interphase chromatin dynamics. *Proc. Natl. Acad. Sci. U. S. A.* **2013**, *110* (39), 15555−15560.
(158) Shaban, H. A.; Barth, R.; Recoules, L.; Bystricky, K. Hi-D: nanoscale mapping of nuclear dynamics in single living cells. *Genome Biol.* **2020**, *21* (1), 95.
(159) Monnier, N.; Guo, S. M.; Mori, M.; He, J.; Lenart, P.; Bathe, M. Bayesian approach to MSD-based analysis of particle motion in live cells. *Biophys. J.* **2012**, *103* (3), 616−626.
(160) Serge, A.; Bertaux, N.; Rigneault, H.; Marguet, D. Dynamic multiple-target tracing to probe spatiotemporal cartography of cell membranes. *Nat. Methods* **2008**, *5* (8), 687−694.
(161) Shaban, H. A.; Friman, E. T.; Deluz, C.; Tollenaere, A.; Katanayeva, N.; Suter, D. M. Individual transcription factors modulate both the micromovement of chromatin and its long-range structure. *Proc. Natl. Acad. Sci. U. S. A.* **2024**, *121* (18), No. e2311374121.
(162) Shaban, H. A.; Seeber, A. Monitoring the spatio-temporal organization and dynamics of the genome. *Nucleic Acids Res.* **2020**, *48* (7), 3423−3434.
(163) Shaban, H. A.; Barth, R.; Bystricky, K. Navigating the crowd: visualizing coordination between genome dynamics, structure, and transcription. *Genome Biol.* **2020**, *21* (1), 278.
(164) Chaudhary, N.; Im, J. K.; Nho, S. H.; Kim, H. Visualizing Live Chromatin Dynamics through CRISPR-Based Imaging Techniques. *Mol. Cells* **2021**, *44* (9), 627−636.

https://doi.org/10.1021/cbmi.4c00033
Chem. Biomed. Imaging 2024, 2, 659−682